3D Modeliranje površinskih voda

Primjer 1. (G. Lončar, GFZG Skripta):
3D model strujanja u pravokutnom bazenu

- 3D numerički model strujanja za pravokutne bazene s duljinom 5000m, širinama 500m i 5000m te s dubinama 10m i 20m.
- strujanje je inducirano homogenim poljem vjetra s brzinama vjetra od 10m/s i 20m/s.
- vjetar se linearno pojačava od inicijalne vrijednosti 0m/s do konačne vrijednosti tijekom perioda „zagrijavanja“ modela od 3600s
- variranje horizontalne i vertikalne rezolucije modelske domene
- nakon postizanja stacionarnog polja strujanja i denivelacije vodnog lica, uspoređuju se vertikalni profili brzine strujanja i kinematskog koeficijent turbulente viskoznosti dobiveni modelom i proračunati temeljem analitičkih (teoretskih) izraza.

1

Korišteni numerički model

- Numerički model Mike 3fm (www.dhigroup.com) temelji se na fleksibilnom diskretizacijskom pristupu
- Njegov hidrodinamički modul numerički rješava 3D Reynolds-ove jednadžbe uz usvajanje Boussinesqove pretpostavke o hidrostatskoj razdiobi tlaka u vertikalnom smjeru.
- Za diskretizaciju jednadžbi se koristi metoda konačnih volumena, bazirana na jednoj ćeliji i podjeli kontinuuma s nepreklapajućim elementima.
- U horizontalnom smjeru korištena je nestrukturirana a u vertikalnom smjeru strukturirana diskretizacija.
- Za izračunavanje konvektivnog toka koristi se približni Riemann-ov solver čime je omogućeno računanje i u slučajevima diskontinuiranih rješenja.
- Za vremensku integraciju se koristi polu-implicitni pristup, gdje se horizontalni parametri tretiraju eksplicitno a vertikalni implicitno.
- Modul turbulencije koristi k-ε formulaciju u vertikalnom smjeru i Smagorinsky koncept u horizontalnom smjeru

2

Modelske domene/mreže

a. 5 km x 0.5 km (fina)
b. 5 km x 0.5 km (gruba)
c. 5 km x 5 km (gruba)

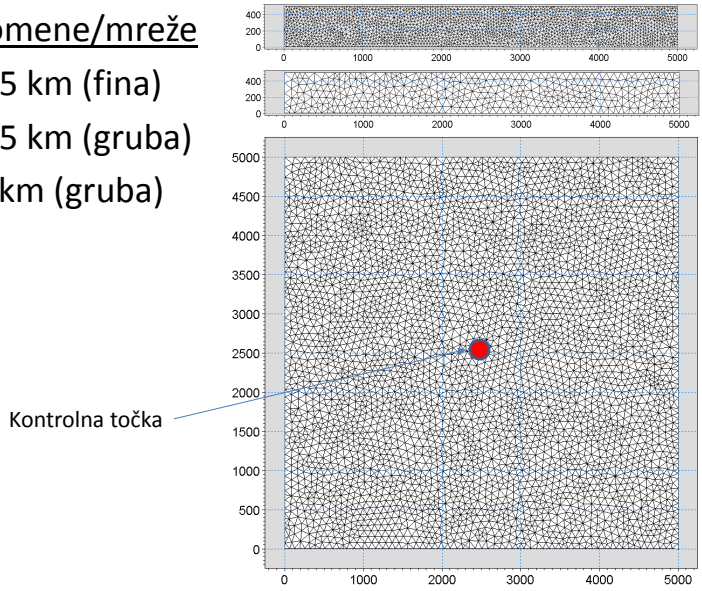

3

Teorijski model

Vjetar uzrokuje površinsko naprezanje τ_s s intenzitetom:

$$\tau_W = \rho_a C_D U_w |U_w| \qquad (2.1)$$

gdje je: ρ_a gustoća zraga (1,23kg/m^3); C_D koeficijent povlačenja vjetra (0.002425); U_W brzine vjetra na 10m od površine. Uz pretpostavku da je dubina bez djelovanja vjetra d znatno veća od denivelacije vodnog lica Δh uzduž simetrale bazena duljine L (uslijed djelovanja vjetra; eng: wind set-up) ravnoteža sila može se napisati u obliku:

$$\rho_0 g d \frac{\Delta h}{L} = \tau_W \qquad (2.2)$$

Na određenoj udaljenosti L od lijevog ruba bazena, uzduž simetrale bazena, očekuje se izdizanje Δh u odnosu na najnižu kotu vodnog lica koja se pojavljuje na lijevom rubu bazena:

$$\Delta h = \frac{\tau_W L}{\rho_0 g d} \qquad (2.3)$$

4

Uslijed djelovanja vjetra formirati će se tzv. baroklini vertikalni profil brzina karakteriziran s površinskim strujama koje prate smjer djelovanja vjetra i kompenzacijskim strujama u dubljim slojevima koje su suprotnog smjera. Profil brzina na određenoj udaljenosti od početka kanala po teoretskom modelu opisan je logaritamskim zakonom:

$$\frac{u}{u_*} = \frac{1}{\kappa}\left(1 + \ln\frac{-z}{h}\right) \qquad (2.3)$$

gdje je: u brzina strujanja na dubini z (gledano od površine); h dubina na poziciji promatranog vertikalnog profila; κ Karmanova konstanta (0,41); $u_*=\max(u_{*W},u_{*B})$ brzinsko naprezanje na površini i dnu $u_{*W} = \sqrt{\tau_W / \rho_0}$; $u_{*B} = \sqrt{\tau_B / \rho_0}$.

Usvajanjem logaritamskog profila brzina moguće je odrediti i vrijednosti kinematskog koeficijenta turbulentne viskoznosti temeljem izraza:

$$\upsilon_T = u_* \kappa h \frac{-z}{h}\left(1 - \frac{-z}{h}\right) \qquad (2.4)$$

5

Numeričke simulacije

analiza	dubina (m)	ρ_o (kg/m^3)	C_D (1)	U_W (m/s)	Δh (m) – teor.	Δh (m) – model
1	10	1,23	0,002425	10	0,008	0,008
2	10	1,23	0,002425	20	0,030	0,032
3	10	1,23	0,002425	10	0,008	0,008
4	10	1,23	0,002425	20	0,030	0,032
5	20	1,23	0,002425	10	0,004	0,004
6	20	1,23	0,002425	20	0,015	0,016
7	10	1,23	0,002425	10	0,008	0,008
8	10	1,23	0,002425	20	0,030	0,032
9	10	1,23	0,002425	10	0,008	0,008
10	10	1,23	0,002425	20	0,030	0,032
11	20	1,23	0,002425	10	0,004	0,004
12	20	1,23	0,002425	20	0,015	0,016
13	10	1,23	0,002425	10	0,008	0,008
14	10	1,23	0,002425	20	0,030	0,032

6

Slika 4.1 Usporedba vertikalnih profila brzina za poziciju kontrolne točke, dobivenih modelom i teoretskim jednadžbama (analize 1,2,3,4,5,6,7,8)

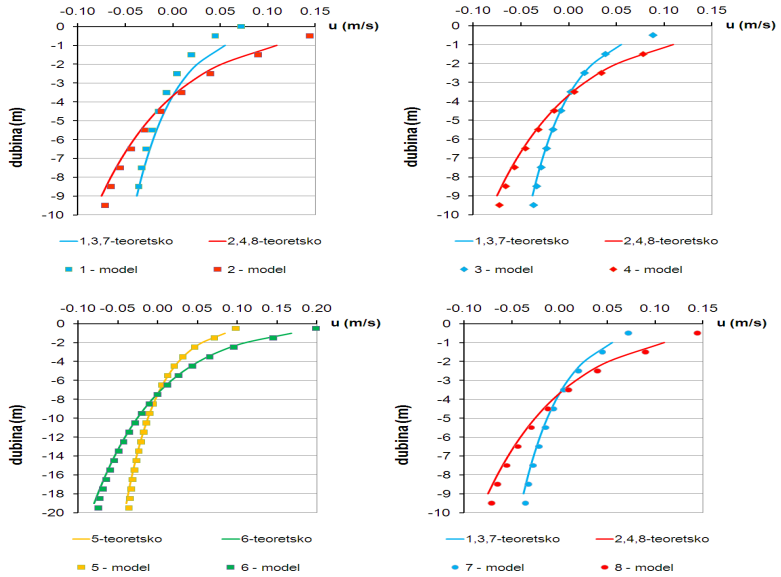

7

Slika 4.2 Usporedba vertikalnih profila kinematskog koeficijenta turbulentne viskoznosti za poziciju kontrolne točke, dobivenih modelom i teoretskim jednadžbama (analize 1,2,3,4,5,6,7,8)

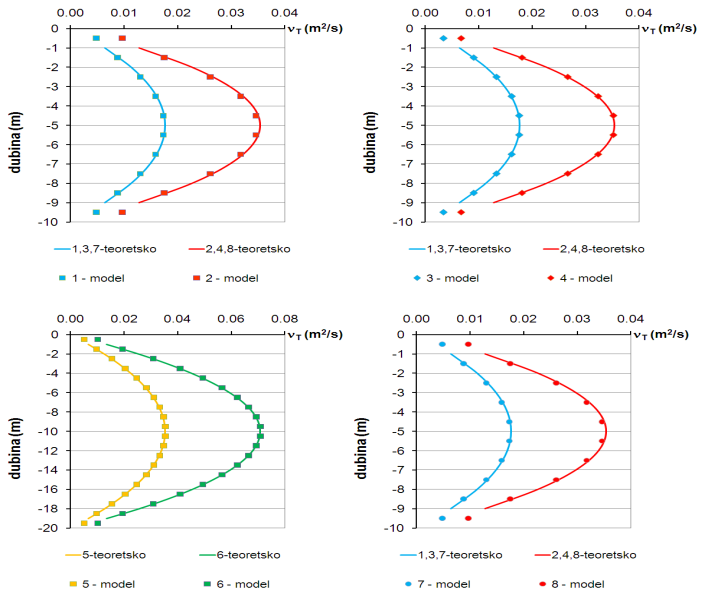

8

Polja brzina za dubine 1, 3, 5, 7 i 9m dobivena analizom 3 (dubina 10m ; brzina vjetra 10m/s)

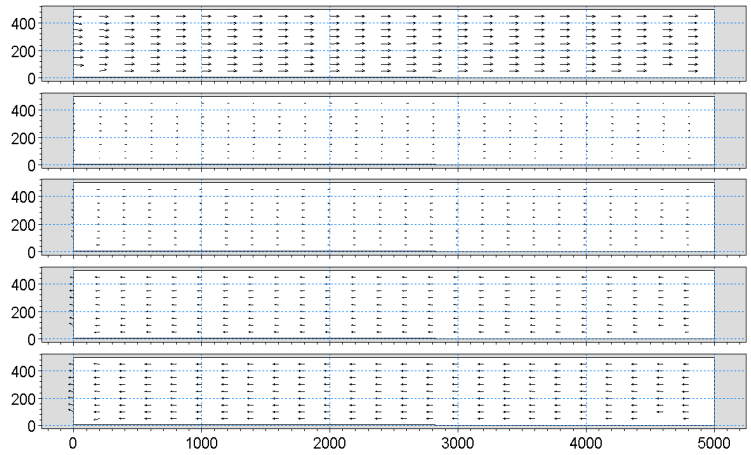

9

Polja brzina za dubine 1, 3, 5, 7 i 9m dobivena analizom 4 (dubina 10m ; brzina vjetra 20m/s)

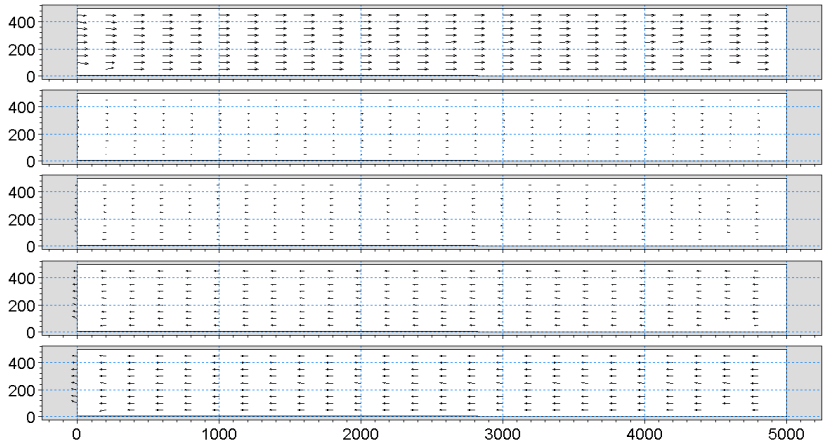

10

3D Modeliranje površinskih voda

Primjer 2. (G. Lončar, GFZG Skripta):
Numerička analiza kvalitete mora na sjevernom Jadranu

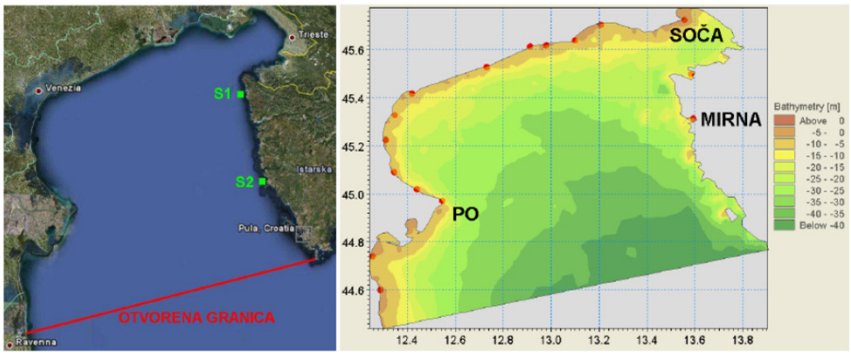

11

Sažetak

Prikazani su rezultati numeričke analize kvalitete mora na području sjevernog Jadrana tijekom razdoblja 1997.-2001. Rubni uvjeti na otvorenoj granici modela i slatkovodni utoci ciklički su ponavljani za polja temperature i saliniteta mora u svim analiziranim godinama. Na kontaktu mora i atmosfere za polja temperature zraka, relativne vlage zraka, naoblake i kratkovalnog zračenja također su korištene ciklički ponavljane vrijednosti. Jedino varijabilno polje u provedenim simulacijama je polje brzine vjetra koje je u analizirano razdoblju definirano temeljem rezultata numeričkog atmosferskog modela Aladin-HR.

Provedenim istraživanjem dobiveni su rezultati koji ukazuju na važnost vjetrovne dinamike kao stohastičkog parametra na kojeg čovjek nema direktan utjecaj i na intenzitet dinamike klorofila-a u području sjevernog Jadrana. Dobiveni rezultati pokazali su da se najveće koncentracije klorofila-a pojavljuju u lipnju i listopadu, a u lipnju 2000. i 2001. godine registrirane su povećane vrijednosti u odnosu na preostale godine iz analiziranog perioda. Razlog ove pojave je vjerojatno duže zadržavanje voda bogatih nutrijentima iz slatkovodnih utoka, primarno iz rijeke Po, u površinskom sloju mora sjeverne Istre.

12

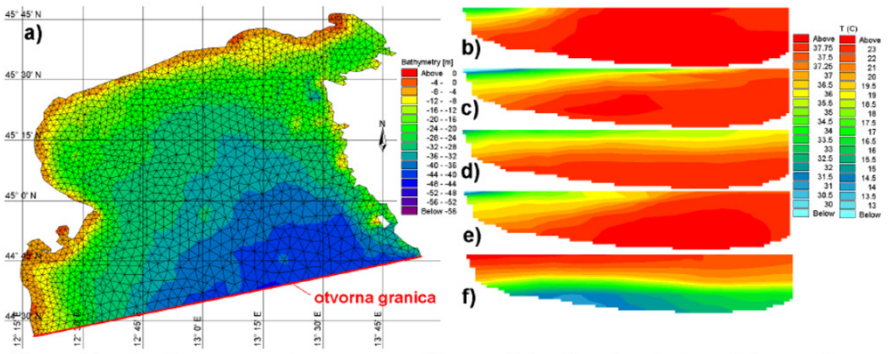

Slika 2 Diskretizacija prostorne domene numeričkog modela Mike 3fm s batimetrijskom podlogom (a), poljima saliniteta (b – zima, c – proljeće, d – ljeto, e – jesen) i poljem temperature mora u vertikalnom profilu otvorene granice (f – ljeto)

13

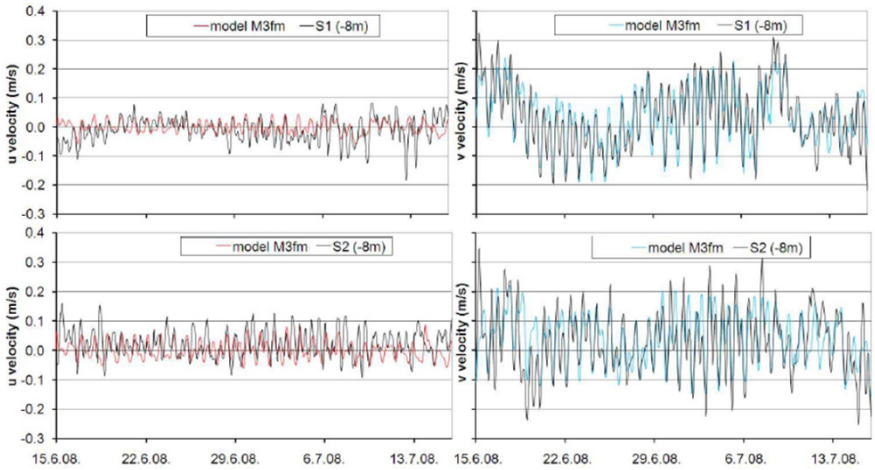

Slika 3 Usporedba izmjerenih i modeliranih (Mike 3fm) satno osrednjenih brzina strujanja na položaju strujomjerne postaje S1 (gore) i S2 (dole) na dubini 8m

14

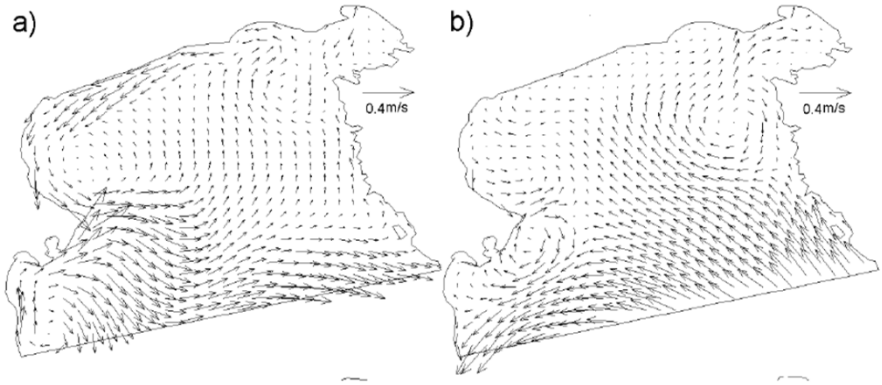

Slika 5 Mjesečno osrednjena polja strujanja na dubini 1m za lipanj (lijevo) i srpanj (desno)

15

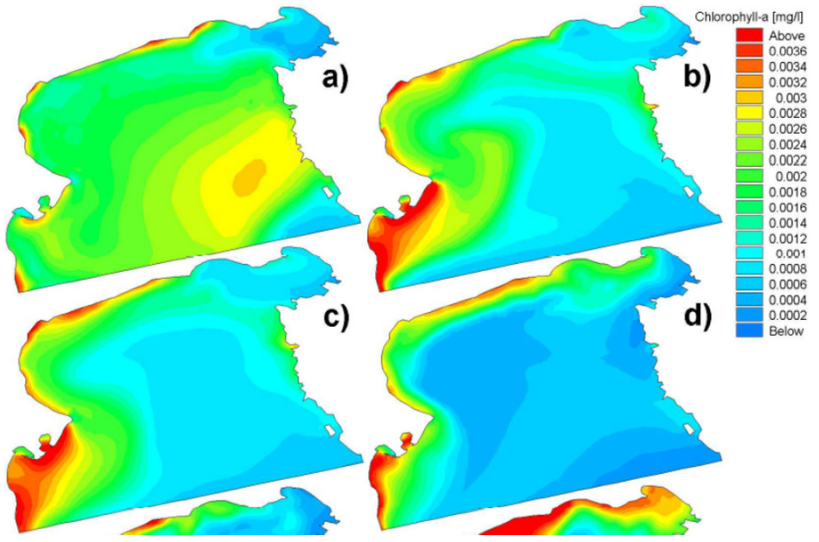

Slika 6 Mjesečno osrednjena polja koncentracija klorofila-a na dubini 1m za lipanj (lijevo) i srpanj (desno) 1997.(a,b), 1999.(c,d), 2000.(e,f) i 2001.(g,h) godine

16

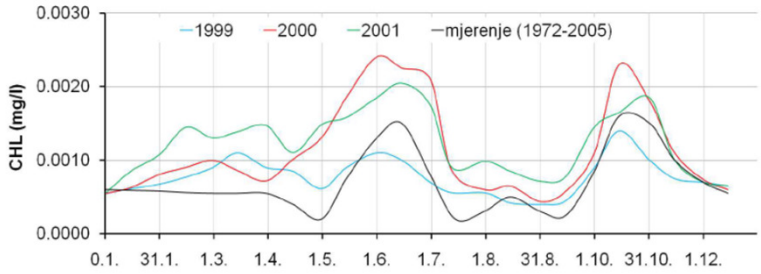

Slika 7 Vremenske serije modelskih koncentracija klorofila-a u površinskom sloju mora sa mjesečno osrednjenim vrijednostima za 1999., 2000. i 2001. godinu na poziciji mjerne postaje S2 i vrijednosti

17

Model dvodimenzionalnog strujanja u otvorenom vodotoku

- U ovom poglavlju opisuje se modelski sustav za analizu dvodimenzionalnog strujanja u kontinuiranoj akvatičkoj sredini poput mora, jezera i rijeka.
- Modelom se definiraju procesne jednadžbe za dvodimenzionalno (u horizontalnoj ravnini) stacionarno ili nestacionarno tečenje nestišljive tekućine te konvektivno diperzivni pronos otopljene ili suspendirane tvari u jednom vertikalnom homogenom sloju uz pretpostavku hidrostatske raspodjele tlaka.
- Sustav jednadžbi sadrži vertikalno integrirane jednadžbe kontinuiteta i očuvanja količine gibanja

18

Jednadžbe – 2D SW

$$\frac{\partial h}{\partial t}+\frac{\partial h\bar{u}}{\partial x}+\frac{\partial h\bar{v}}{\partial y}=hS \tag{7.1}$$

$$\frac{\partial h\bar{u}}{\partial t}+\frac{\partial h\bar{u}^2}{\partial x}+\frac{\partial h\overline{uv}}{\partial y}= \\ =f\bar{v}h-gh\frac{\partial \eta}{\partial x}-\frac{h}{\rho_0}\frac{\partial p_a}{\partial x}-\frac{gh^2}{2\rho_0}\frac{\partial \rho}{\partial x}+\frac{\tau_{SX}}{\rho_0}-\frac{\tau_{BX}}{\rho_0}+\frac{1}{\rho_0}\left[\frac{\partial}{\partial x}(hT_{xx})+\frac{\partial}{\partial y}(hT_{xy})\right]+hu_SS \tag{7.2}$$

$$\frac{\partial h\bar{v}}{\partial t}+\frac{\partial h\overline{uv}}{\partial x}+\frac{\partial h\bar{v}^2}{\partial y}= \\ =-f\bar{u}h-gh\frac{\partial \eta}{\partial y}-\frac{h}{\rho_0}\frac{\partial p_a}{\partial y}-\frac{gh^2}{2\rho_0}\frac{\partial \rho}{\partial y}+\frac{\tau_{SY}}{\rho_0}-\frac{\tau_{BY}}{\rho_0}+\frac{1}{\rho_0}\left[\frac{\partial}{\partial x}(hT_{YX})+\frac{\partial}{\partial y}(hT_{YY})\right]+hv_SS \tag{7.3}$$

gdje je: τ_{sx}, τ_{sy} naprezanja na površini; τ_{bx}, τ_{by} naprezanja na dnu; T_{xx}, T_{xy}, T_{yy} lateralna naprezanja; S intenzitet ponora ili izvora; u_S, v_S komponente brzine u x i y smjeru na mjestu izvora; D_x, D_y koeficijenti disperzije u x i y smjeru.

19

Površinsko naprezanje pri djelovanju s dnom (trenje sa dnom) definirano je jednadžbom 7.4:

$$\tau_{bX}=\frac{\rho g\bar{u}|\bar{u}|}{C^2} \quad ; \quad \tau_{bY}=\frac{\rho g\bar{v}|\bar{v}|}{C^2} \tag{7.4a,b}$$

gdje je: C Chezyjev koeficijent ($C = (1/M)\, h^{1/6}$; M -Manningov koeficijent hrapavosti);

Površinsko naprezanje uzrokovano djelovanjem vjetra opisano je empiričkim jednad. 6.7:

$$\tau_{sx} = \rho_a\, C_D\, U_{wX}\, |\, U_{wX}\, | \quad ; \quad \tau_{sy} = \rho_a\, C_D\, U_{wY}\, |\, U_{wY}\, | \tag{6.7a,b}$$

gdje je: ρ_a gustoća zraka; C_D koeficijent povlačenja vjetra; U_{WX}, U_{WY} komponente brzine vjetra na 10m od površine.

20

Lateralnim naprezanjima T_{XX}, T_{XY}, T_{YY} u jednadžbama količine gibanja obuhvaćeni su utjecaji turbulentne količine gibanja, usrednjavanja brzina po vertikali i fluktuacija na podinkrementalnom prostornom modelskom mjerilu temeljem formulacije efektivnog kinematskog koeficijenta turbulentne viskoznosti E. Njime se omogućuje prigušenje oscilacija kratkih valova i reprodukcija efekata vezanih na podinkrementalno mjerilo.

$$T_{XX} = E\frac{\partial \bar{u}}{\partial x} \quad ; \quad T_{XY} = \frac{1}{2}E\left(\frac{\partial \bar{u}}{\partial y} + \frac{\partial \bar{v}}{\partial x}\right) \quad ; \quad T_{YY} = E\frac{\partial \bar{v}}{\partial y} \tag{7.6}$$

$$E = C_{sm}^2 l^2 \left[\left(\frac{\partial \bar{u}}{\partial x}\right)^2 + \frac{1}{2}\left(\frac{\partial \bar{u}}{\partial y} + \frac{\partial \bar{v}}{\partial x}\right)^2 + \left(\frac{\partial \bar{v}}{\partial y}\right)^2\right]^{1/2} \tag{7.7}$$

gdje je: l udaljenost između dva proračunska čvora modela a C_{sm} modelska konstanta korištene Smagorinski formulacije.

21

Jednadžba konvektivno-disperzivnog pronosa za salinitet i temperaturu definirane su sljedećim jednadžbama:

$$\frac{\partial}{\partial t}\left(h\bar{T}\right) + \frac{\partial}{\partial x}\left(\bar{u}h\bar{T}\right) + \frac{\partial}{\partial x}\left(\bar{v}h\bar{T}\right) = \frac{\partial}{\partial x}\left(h \cdot D_X \cdot \frac{\partial \bar{T}}{\partial x}\right) + \frac{\partial}{\partial y}\left(h \cdot D_Y \cdot \frac{\partial \bar{T}}{\partial y}\right) + h\hat{H} + hT_S S \tag{7.7}$$

$$\frac{\partial}{\partial t}\left(h\bar{S}\right) + \frac{\partial}{\partial x}\left(\bar{u}h\bar{S}\right) + \frac{\partial}{\partial x}\left(\bar{v}h\bar{S}\right) = \frac{\partial}{\partial x}\left(h \cdot D_X \cdot \frac{\partial \bar{S}}{\partial x}\right) + \frac{\partial}{\partial y}\left(h \cdot D_Y \cdot \frac{\partial \bar{S}}{\partial y}\right) + hS_S S \tag{7.8}$$

gdje je: $\bar{T}$ i $\bar{S}$ vertikalno osrednjene temperature i salinitet; T_S i S_S temperatura i salinitet izvora.

22

U vektorskoj formi:

$$\frac{\partial H}{\partial t} + \nabla \bullet hV + q = 0$$

$$\frac{\partial V}{\partial t} + V \bullet \nabla V = -g\nabla H + \nu_t \nabla^2 V - c_f V + fk \times V$$

lokalna akceleracija | konvektivna akceleracija | barotropični tlak | turbulentna difuzija | trenje sa dnom | Coriolis

23

Rubni uvjeti

a. Zadana razina vodnog lica $H = H_b$

a. Zadani nagib vodnog lica $\nabla H \bullet n = S_b$

a. Zadani protok $\iint_b V \bullet n \, dS = Q_b$

24

Model jednodimenzionalnog strujanja u otvorenom vodotoku

- U ovom poglavlju opisuje se modelski sustav za analizu jednodimenzionalnog strujanja u prirodnim ili umjetnim vodotocima
- Modelom se definiraju procesne jednadžbe za jednodimenzionalno (u dominantnom smjeru tečenja) stacionarno ili nestacionarno tečenje nestišljive tekućine te konvektivno diperzivni pronos otopljene ili suspendirane tvari u poprečnom presjeku uz pretpostavku hidrostatske raspodjele tlaka.
- Sustav jednadžbi sadrži jednadžbe kontinuiteta i očuvanja količine gibanja integrirane po površini poprečnog presjeka

25

1D Model riječnog sliva

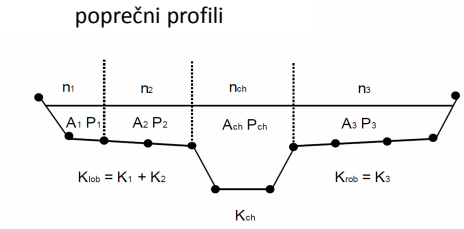

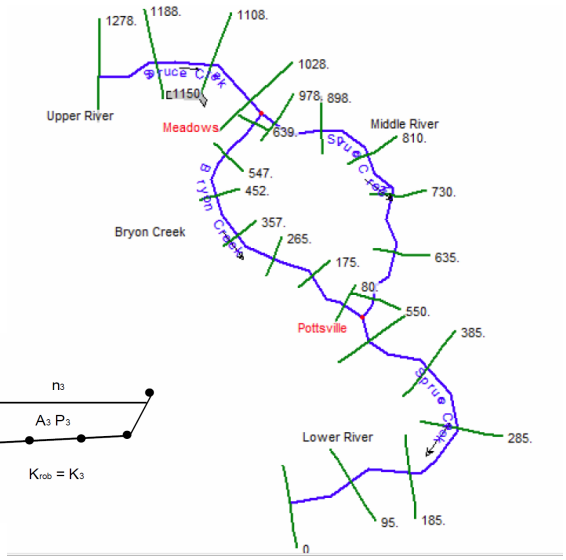

26

Korito + inundacije

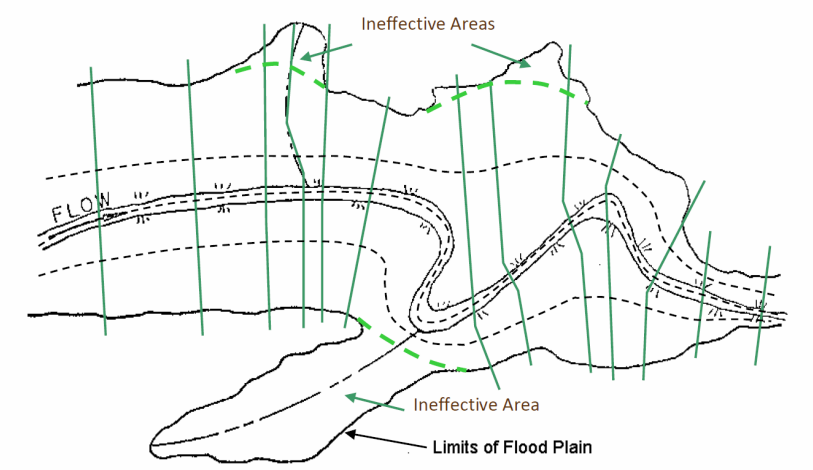

27

Izvod jednadžbi (nestacionarno tečenje)

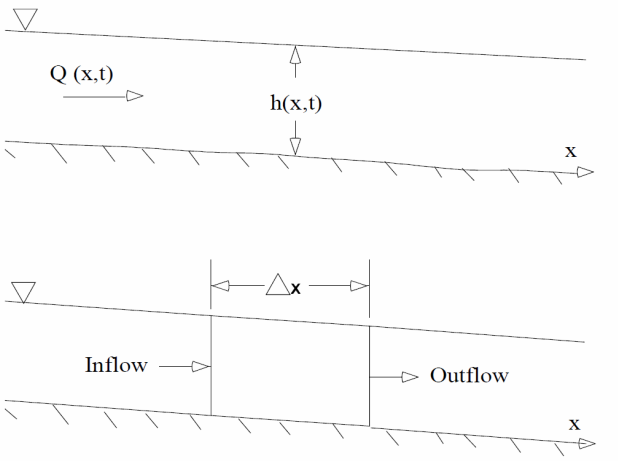

28

Zakon o očuvanju mase (jednadžba kontinuiteta)

$$\rho \frac{\partial A_T}{\partial t} \Delta x = \rho \left[\left(Q - \frac{\partial Q}{\partial x} \frac{\Delta x}{2} \right) - \left(Q + \frac{\partial Q}{\partial x} \frac{\Delta x}{2} \right) + Q_l \right]$$

$$\frac{\partial A_T}{\partial t} + \frac{\partial Q}{\partial x} - q_l = 0$$

ρ = gustoća, A_T = površina, Q = protok, $Q_L = q_l \Delta x$ = bočni dotok

29

Zakon o očuvanju količine gibanja (2. Newtonov zakon)

$$\sum F_x = \frac{d\vec{M}}{dt}$$

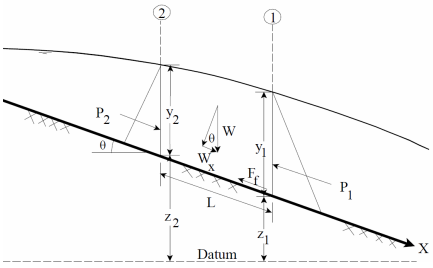

$$\rho \Delta x \frac{\partial Q}{\partial t} = -\rho \frac{\partial QV}{\partial x} \Delta x - \rho g A \frac{\partial h}{\partial x} \Delta x - \rho g A \frac{\partial z_0}{\partial x} \Delta x - \rho g A S_f \Delta x$$

lokalna akceleracija | konvektivna akceleracija | razlika tlaka | gravitacija | trenje sa dnom

$$\frac{\partial Q}{\partial t} + \frac{\partial QV}{\partial x} + gA \left(\frac{\partial z}{\partial x} + S_f \right) = 0$$

ρ = gustoća, A = površina, Q = protok, V = brzina, g=grav. akc., z = razina dna, Sf =

30

St. Venantove jednadžbe

$$\frac{\partial A_T}{\partial t} + \frac{\partial Q}{\partial x} - q_l = 0$$

2 jednadžbe za h(x,t) ili z(x,t) i Q(x,t)

$$\frac{\partial Q}{\partial t} + \frac{\partial QV}{\partial x} + gA\left(\frac{\partial z}{\partial x} + S_f\right) = 0$$

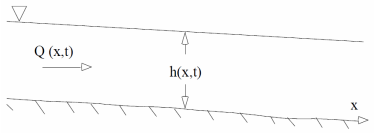

$$z = z_0 + h$$

$$S_f = \frac{Q|Q|n^2}{R^{4/3}A^2}$$

Iz geometrije poprečnog presjeka

z_0 = kota dna
A=A(h) = površina presjeka
P=P(h) = omočeni obod
R=A/P = hidraulički radijus

31

Modeliranje rijeka

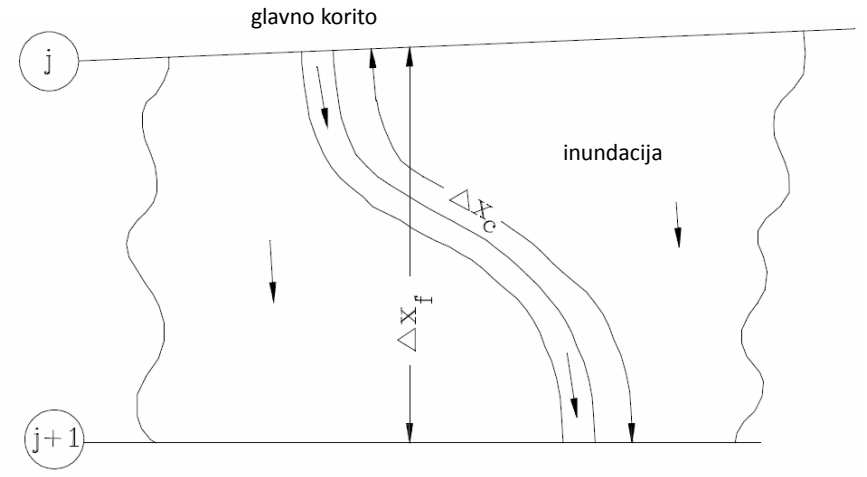

32

Uz pretpostavku za omjer protoka u koritu i inundaciji:

$$\frac{\partial A}{\partial t}+\frac{\partial(\Phi Q)}{\partial x_c}+\frac{\partial[(1-\Phi)Q]}{\partial x_f}=0$$

$$\frac{\partial Q}{\partial t}+\frac{\partial\left(\Phi^2 Q^2/A_c\right)}{\partial x_c}+\frac{\partial\left((1-\Phi)^2 Q^2/A_f\right)}{\partial x_f}+gA_c\left[\frac{\partial Z}{\partial x_c}+S_{fc}\right]+gA_f\left[\frac{\partial z}{\partial x_f}+S_{ff}\right]=0$$

$$\phi = K_c/\left(K_c+K_f\right)$$

$$K=\frac{1.486}{n}AR^{2/3}$$

33

Rubni i početni uvjeti

- Uzvodni rubni: uobičajeno zadani Q(0,t)
- Nizvodni rubni:
  a. Zadani h(L,t) - nivogram
  b. Zadani Q(L,t) - hidrogram
  c. Zadani Q(h) – konsumpcijska krivulja
  d. Normalna dubina:

$$S_o = \frac{Q|Q|n^2}{R^{4/3}A^2}$$

nagib dna

- Početni: zadani h(x,0) i Q(x,0)

34

1D Stacionarno tečenje

$$\cancel{\frac{\partial Q}{\partial t}} + \frac{\partial QV}{\partial x} + gA\left(\frac{\partial z}{\partial x} + S_f\right) = 0$$

$$AV\frac{dV}{dx} + gA\left(\frac{dz}{dx} + S_f\right) = 0$$

$$\frac{d}{dx}\left(z + \frac{V^2}{2g}\right) = -S_f$$

ukupna energetska visina

gubitak mehaničke energije uslijed trenja

35

Metoda standardnog koraka

$$Z_2 + Y_2 + \frac{a_2 V_2^2}{2g} = Z_1 + Y_1 + \frac{a_1 V_1^2}{2g} + h_e$$

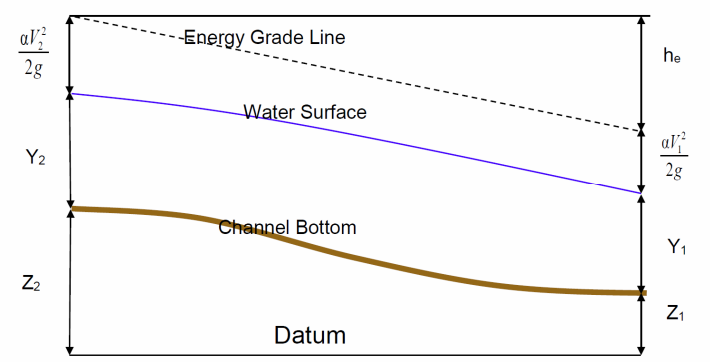

36

Manningova jednadžba

$$Q = KS_f^{1/2}$$

$$K = \frac{1}{n} AR^{2/3}$$

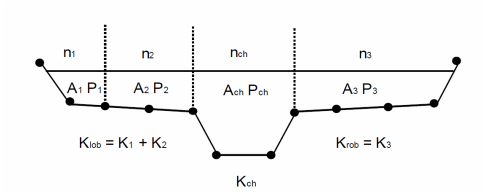

$$n_c = \left[\frac{\sum_{i=1}^{N} \left(P_i n_i^{1.5} \right)}{P} \right]^{2/3}$$

37

koeficijent lokalnog gubitka

$$h_e = L\overline{S}_f + C\left| \frac{a_2 V_2^2}{2g} - \frac{a_1 V_1^2}{2g} \right|$$

gubitak energije

$$L = \frac{L_{lob}\overline{Q}_{lob} + L_{ch}\overline{Q}_{ch} + L_{rob}\overline{Q}_{rob}}{\overline{Q}_{lob} + \overline{Q}_{ch} + \overline{Q}_{rob}}$$

$$\alpha = \frac{(A_t)^2 \left[\frac{K_{lob}^3}{A_{lob}^2} + \frac{K_{ch}^3}{A_{ch}^2} + \frac{K_{rob}^3}{A_{rob}^2} \right]}{K_t^3}$$

$$\overline{S}_f = \left(\frac{Q_1 + Q_2}{K_1 + K_2} \right)^2$$

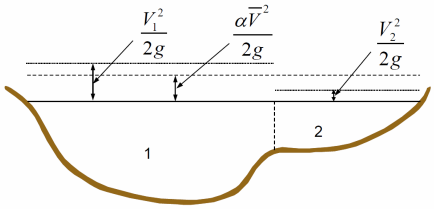

$$\alpha \frac{\overline{V}^2}{2g} = \frac{Q_1 \frac{V_1^2}{2g} + Q_2 \frac{V_2^2}{2g}}{Q_1 + Q_2}$$

38

Hydrologic Engineering Center (CEIWR-HEC) Suite of Software

U.S. Army Corps of Engineers (USACE)
BUILDING STRONG®

Mission

- Mission focus emphasizes the primary need to serve the USACE engineering practitioners at the field level and to enable USACE to successfully accomplish civil works studies, projects and operations.
- CEIWR-HEC software, methods and related products have become the world's standard and CEIWR-HEC software has become synonymous with hydrologic and hydraulic engineering analysis.
- Software is used worldwide for five major reasons: exceptional software; fully supported/maintained; documentation; training; availability.
- The Center's suite of software includes applications that are supported by a library of utility programs, which includes Geographic Information System (GIS) support.
- Additional information about CEIWR-HEC and its software is available on the CEIWR-HEC web site at www.hec.usace.army.mil.

39

HEC Software

- CWMS
- HEC-DSSVue
- HEC-EFM
- HEC-FDA
- HEC-FIA
- HEC-GeoEFM
- HEC-GeoHMS
- HEC-GeoRAS
- HEC-GridUtil
- HEC-HMS
- HEC-LifeSim
- HEC-RAS
- HEC-ResPRM
- HEC-ResSim
- HEC-RPT
- HEC-RTS
- HEC-SSP
- HEC-WAT

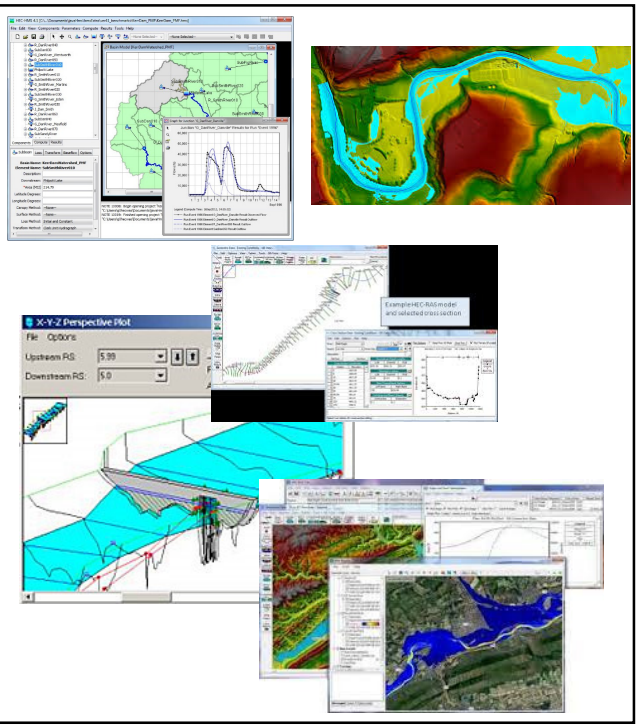

40

Hydrologic Modeling System (HEC-HMS)

- Computes streamflow throughout a river basin given precipitation and watershed characteristics.
- Event & continuous simulation, multiple routing/ runoff methods, gridded precipitation, losses & runoff, snowmelt, dam break.
- Represent a wide range of hydrologic systems, from large river basin water supply & flood hydrology, to small urban or natural watershed runoff.
- Industry standard hydrologic modeling tool that is used worldwide. Used by all USACE District & Division offices. Certified for FEMA studies. Adopted by multiple agencies.

41

River Analysis System (HEC-RAS)

- Computes river velocities, stages, profiles, and inundated areas given streamflow & geometry.
- Steady & Unsteady Flow; Sediment Transport; Water Quality & Temperature.
- Industry standard hydraulic tool that is used worldwide. Used by all USACE District & Division offices. Important tool for dam and levee safety studies.
- NWS, NRCS, USGS and FHWA have adopted HEC-RAS for one-dimensional river hydraulics modeling. Eighty percent of FEMA Floodplain/ Floodway analyses are performed with HEC-RAS.
- Two-dimensional capabilities are available.

42

Reservoir System Simulation (HEC-ResSim)

- Simulates reservoir operations for flood management, low flow augmentation & water supply for planning studies, detailed reservoir regulation plan investigations, and real-time decision support.
- Coupled with CE-QUAL-W2 for water quality.
- Quickly becoming industry standard.
- Used domestically and internationally.

Flood Damage Reduction Analysis, HEC-FDA

- Software to perform flood risk management analyses; plan evaluation and plan formulation Tool.
- Compare plans using Expected Annual Damage (EAD) damage reduction benefits & project performance.
- Certified through PMIP 2009. Since 1996, HEC-FDA uses risk analysis procedures.
- Used by all USACE District & Division offices for performing flood risk management analysis. Most widely used planning tool for plan formulation/alternative analysis.
- Helps answer the question "Which proposed flood damage reduction plan is the best from an economic standpoint"?

43

Flood Impact Analysis, HEC-FIA

- Software to perform project benefit analysis including loss-of-life consequences; evaluate flood risk management measures (structural and non-structural) using risk and uncertainty and including systems approach and GIS capability.
- Computes damages to structures and other contents of the floodplain (including agricultural and environmental) given river stages & damage relationships. Also computes Loss-of-Life.
- Used extensively for dam & levee safety studies.
- Impact Response Report useful to Emergency Management Operations.

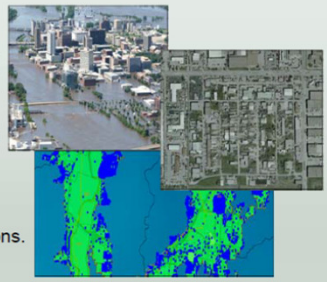

Ecosystems Function Model, HEC-EFM

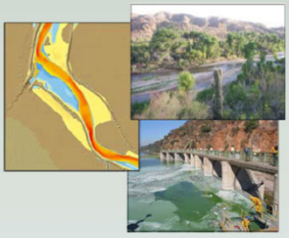

- Planning tool for use in ecosystem restoration and water resources management.
- Evaluates habitat provided by restoration alternatives & ecosystem responses to reservoir management decision-making.
- Aligns with other hydrologic & hydraulic models to perform environmental benefits analyses as part of decision support systems.
- Has been used to assess floodplain reconnections, drought contingency planning, stream restoration, dam removal, endangered species management, reservoir reoperations, and environmental flow analyses.
- Certified through USACE PMIP in 2013.

44

Hydrologic Engineering Center (CEIWR-HEC) River Analysis System (HEC-RAS)

Description

The U.S. Army Corps of Engineers' Hydrologic Engineering Center (CEIWR-HEC), River Analysis System (HEC-RAS) is an integrated system of software, designed for interactive use in a multitasking environment. The software allows simulation of one-dimensional steady and unsteady flow river hydraulics, water surface profile calculations and inundation mapping. HEC-RAS is comprised of a graphical user interface (GUI), separate hydraulic analysis components, data storage and management capabilities, graphics and reporting facilities.

45

Existing Capabilities

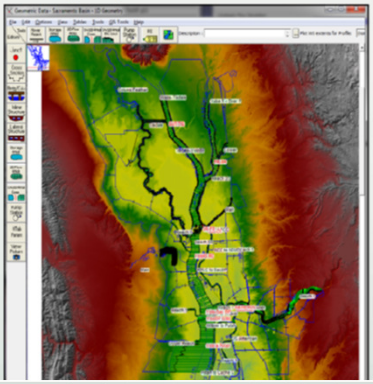

- **Analysis Features** - steady flow water-surface profiles; one- & two-dimensional unsteady flow hydrodynamic simulations; movable boundary sediment transport computations; and water quality analysis (temperature modeling and constituent transport utilizing the Nutrient Sub-Module (NSM) library). Additionally, options are available for: detailed hydraulic structure modeling (spillways, gates, weirs, bridges, culverts, and pump stations); dam & levee breaching, navigation dam operations; U.S. Federal Emergency Management Agency (FEMA) floodway encroachments; split flow optimization; sediment transport capacity & bridge scour; channel modifications; mixed flow regime; sediment budget analysis; ice cover & ice jams; and, model calibration features.
- **Geometric Features** - bridge hydraulics; extensive culvert hydraulics (nine types of culverts); multiple opening analysis (bridges & culverts); inline structures (spillways, gates & weirs); lateral structures (gates, weirs, culverts, & rating curves); two-dimensional flow areas; storage/ponding areas; hydraulic connections between two-dimensional flow & storage areas; pumping stations; floating ice; levees; extensive data import and export; and, geographic information system (GIS) connections.
- **Graphical Output** - water surface profile plots; cross sections; rating curves; stage and flow hydrographs; generalized profile plot of any variable (i.e., velocity); three-dimensional view of river system; and, graphical animations. Inundation mapping & spatial displays of model output are available directly from within HEC-RAS using the RAS-Mapper tool (since Version 4.1).
- **Tabular Output** - detailed output tables for cross sections & all structures, summary output tables, and user defined output.

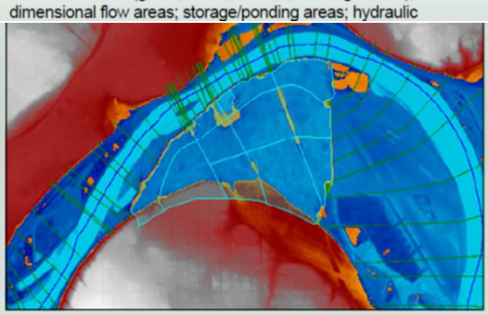

46

Applications

HEC-RAS users include: all USACE District & Division Offices; USDA Natural Resources Conservation Service (NRCS) & Federal Highway Administration (FHWA) which has adopted use in one-dimensional river hydraulics analysis; other Federal agencies including FEMA, U.S. Geological Survey (USGS), U.S. Bureau of Reclamation (USBR), National Weather Service (NWS), Fish & Wildlife; state & local governments; private industry; environmental organizations, universities, and engineers worldwide.

Projects

- **Ohio & Mississippi Rivers** - model of the entire Ohio River System, a portion of the Mississippi River, and most major tributaries. The model has been developed for real-time river forecasting & is jointly used with the NWS. HEC-RAS modeling provided direct support for the Ohio/Mississippi river flooding that occurred in 2011.
- **Red River of the North** - HEC-RAS models have been developed for the entire Red River of the North for planning analysis studies. The models were also used this year during the spring snow melt runoff, for decision support.
- **Columbia River & Tributaries** - general flood damage reduction analysis & real-time forecasting. HEC-RAS is currently being used for real-time forecasting of the Spring flood runoff on the Columbia River.
- **Mississippi River** - one-dimensional unsteady flow models by all Districts along the river
- **Susquehanna River, PA** - flood warning system & FEMA mapping
- **Truckee River, NV** - flood damage reduction analysis & ecosystems evaluation
- **Anacostia River, MD** - flood damage reduction
- **Jefferson Parish, LA** - highly urban interconnected canals & pump systems
- **East Branch of the California State Water Project (SWP)** - being used in study on enlarging the SWP
- **New Orleans Interior Flooding Analysis - Hurricane Katrina Study**

47

HEC-RAS 1D stacionarno

Primjer 1: Uspor (*backwater*) – usporedba sa ručnim izračunom

Table 2-1. Specifications for the One-Dimensional Backwater Test Case

Parameter	Value
Bottom width, b (feet)	20
Side slopes, z	2:1 H:V
Bed slope, S	0.0016
Roughness, n	0.025
Flow rate, Q cfs (cubic feet per second)	400
Downstream Boundary Condition, WS (feet)	5.0

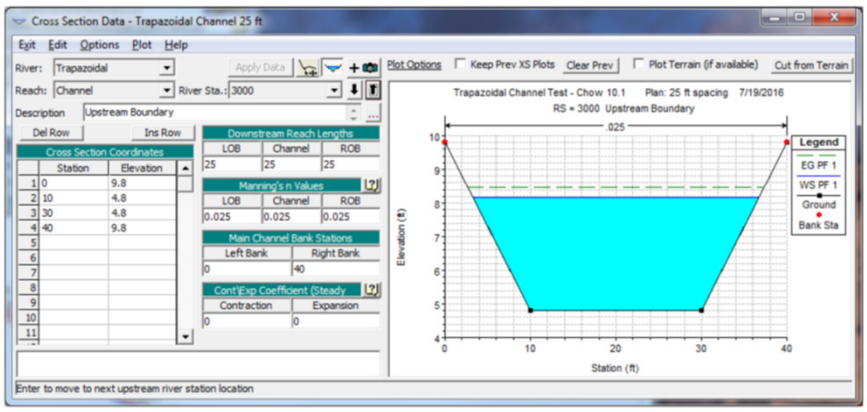

48

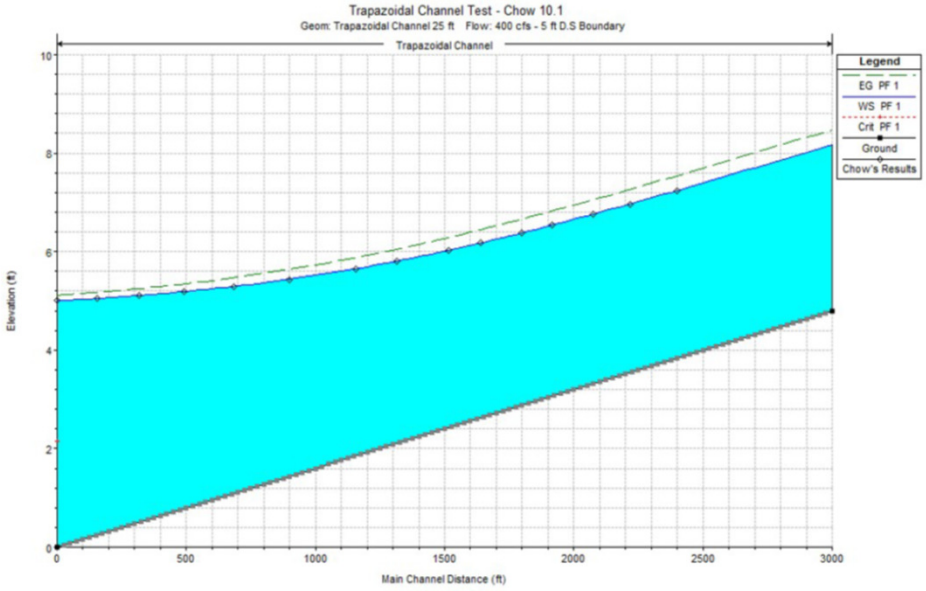

Figure 2-2. HEC-RAS Computed versus Hand Calculations from Chow (1959)

49

HEC-RAS 1D stacionarno

Primjer 2: Tečenje preko izbočine – tranzicija režima

$$z_b = \begin{cases} 0, & \text{for } x < 8 \\ 0.2 - 0.05(x-10)^2, & \text{for } 8 \le x < 12 \\ 0, & \text{for } 12 \le x \end{cases}$$

Table 2-2. Specifications for the One-Dimensional Transcritical Flow over a Bump without Friction Test Case

Parameter	Value
Bottom width, b (meter)	0.3
Side slopes, z	0.0
Bed slope, S	0.0
Roughness, frictionless, n	0.0001
Flow rate, Q cms (cubic meter per second)	0.054
Downstream Boundary Condition, WS (meter)	0.33

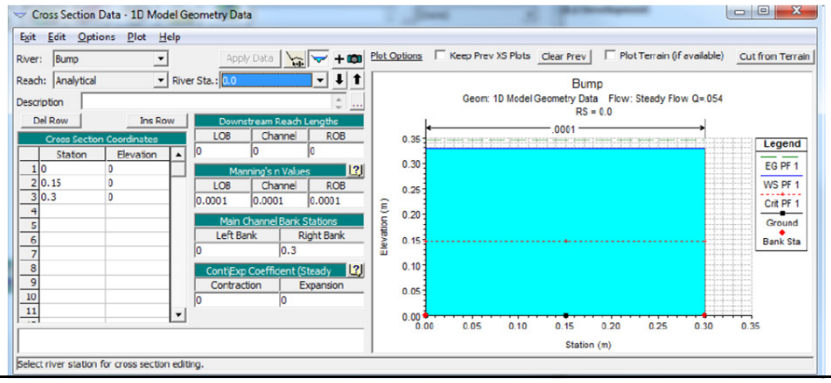

50

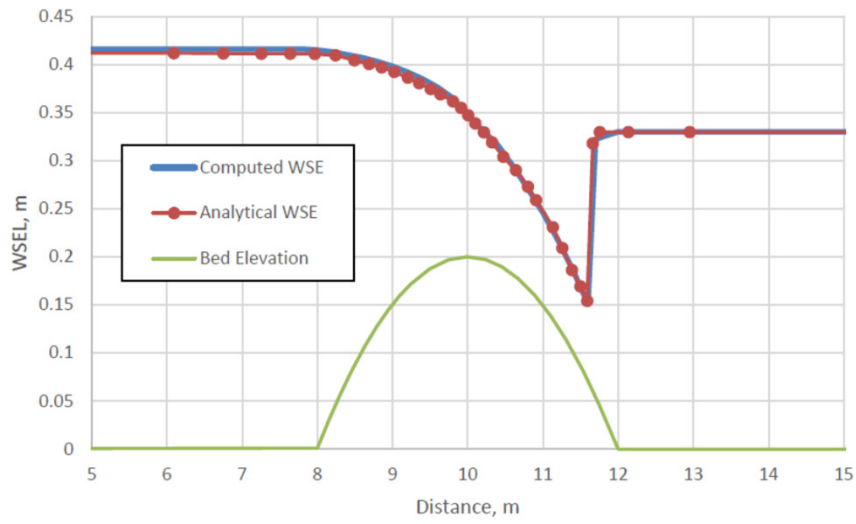

Figure 2-4. Computed and Analytical Solution of a Mixed Flow Regime Problem

51

HEC-RAS 1D stacionarno

Primjer 3: Tečenje preko stepenice (*drop structure*)

Table 2-3. Cross Section Spacing for the HEC-RAS Model

Location	Reach Lengths (feet)
Upstream of drop structure	10
Over the drop	2
Inside the stilling basin	10
Downstream of structure	10

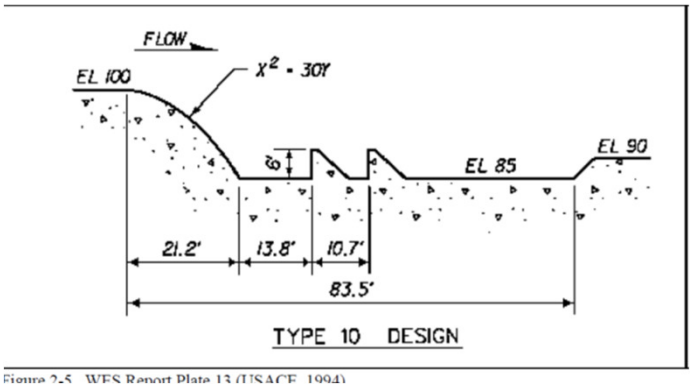

Figure 2-5. WES Report Plate 13 (USACE, 1994)

52

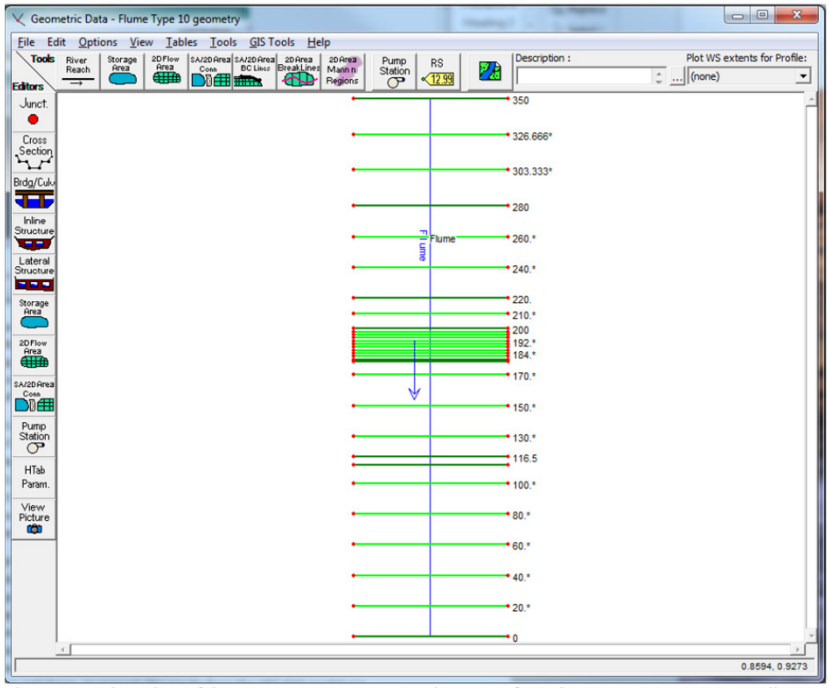

Figure 2-6. Plan View of the Drop Structure's Geometric Layout from the HEC-RAS Geometry Editor

53

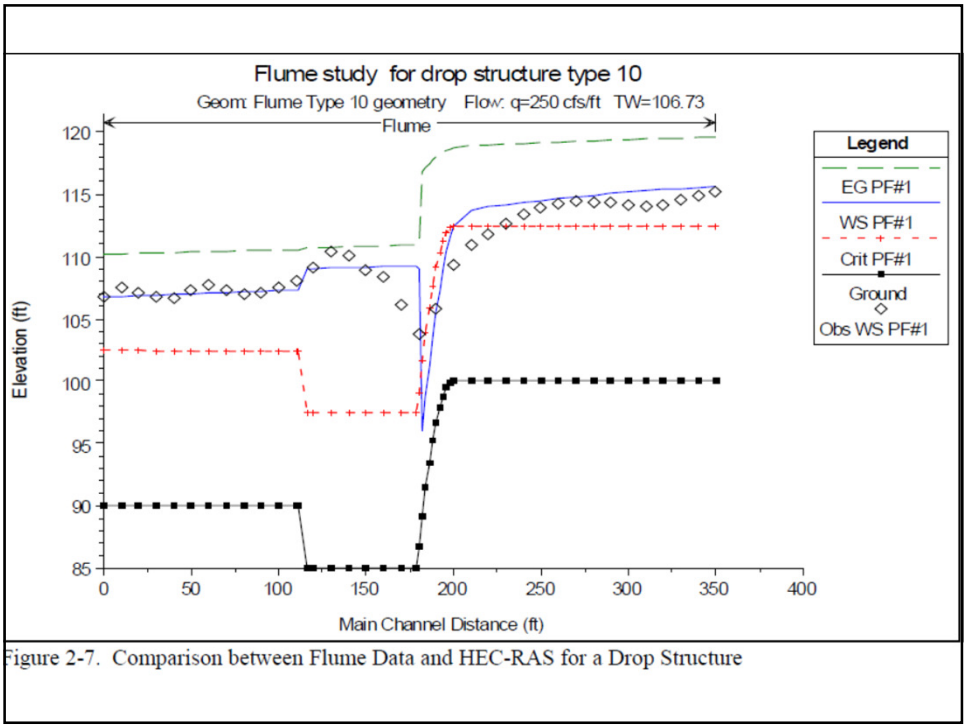

Figure 2-7. Comparison between Flume Data and HEC-RAS for a Drop Structure

54

HEC-RAS 1D nestacionarno

Primjer 1: St. Joaquin Canal

Table 3-2. Specifications for the San Joaquin Canal Test Case

Parameter	Value
Bottom width, b (feet)	40
Side slopes, z	1.5:1 H:V
Bed slope, S	0.00005
Roughness, n	0.012
Flow rate, Q cfs	1,700 to 0.0
Downstream Gated Structure, Gate Openings (feet)	2.6 to 0.0
Downstream Boundary Condition, WS (feet)	219.8

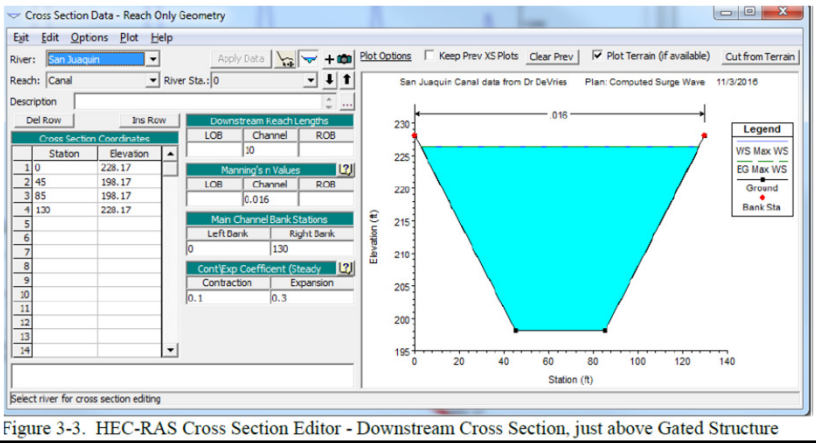

Figure 3-3. HEC-RAS Cross Section Editor - Downstream Cross Section, just above Gated Structure

55

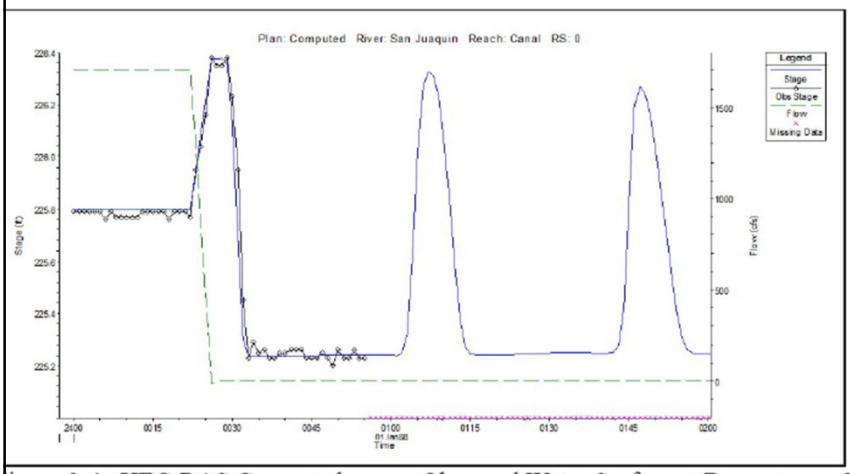

igure 3-4. HEC-RAS Computed versus Observed Water Surface at Downstream Station 0.0

56

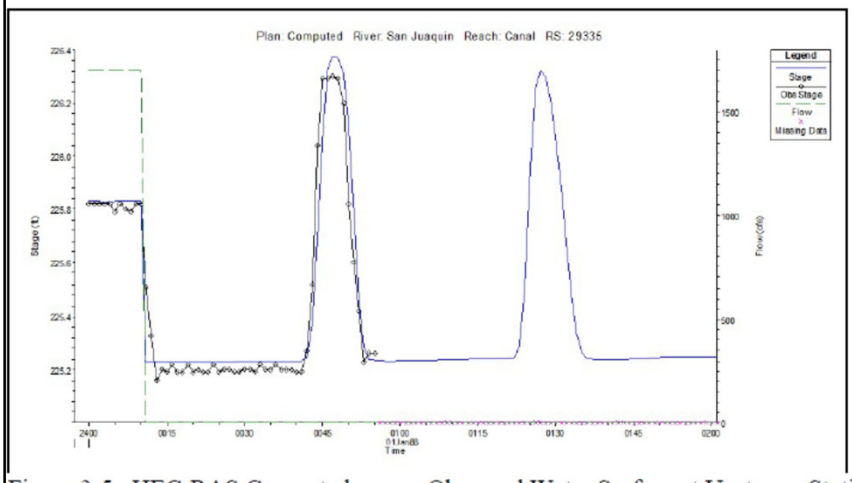

Figure 3-5. HEC-RAS Computed versus Observed Water Surface at Upstream Station 29335

57

HEC-RAS 1D nestacionarno

Primjer 2: Columbia River

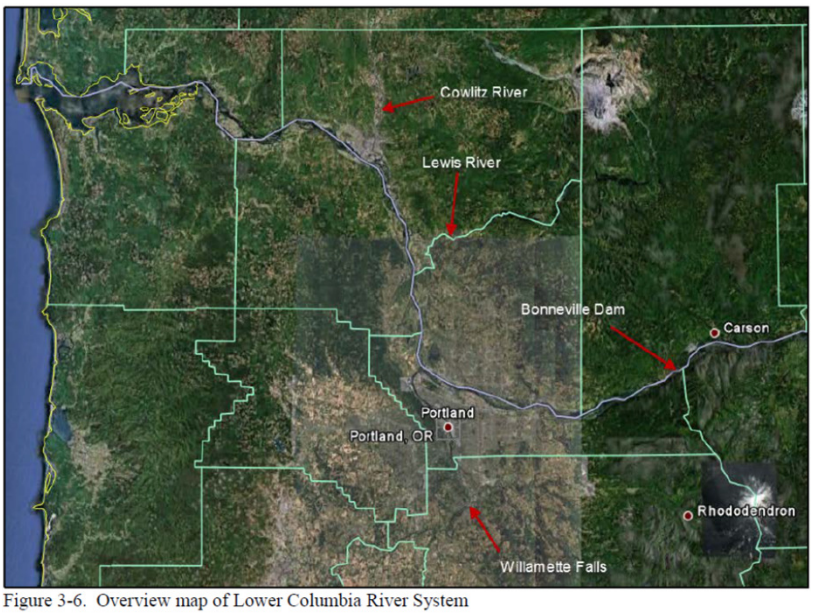

Figure 3-6. Overview map of Lower Columbia River System

58

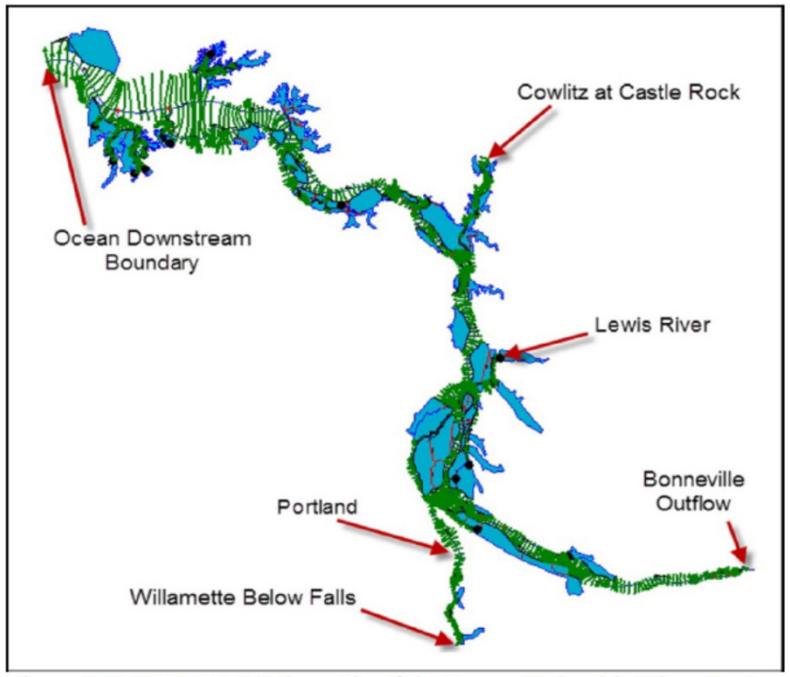

Figure 3-7. HEC-RAS Schematic of the Lower Columbia River System

59

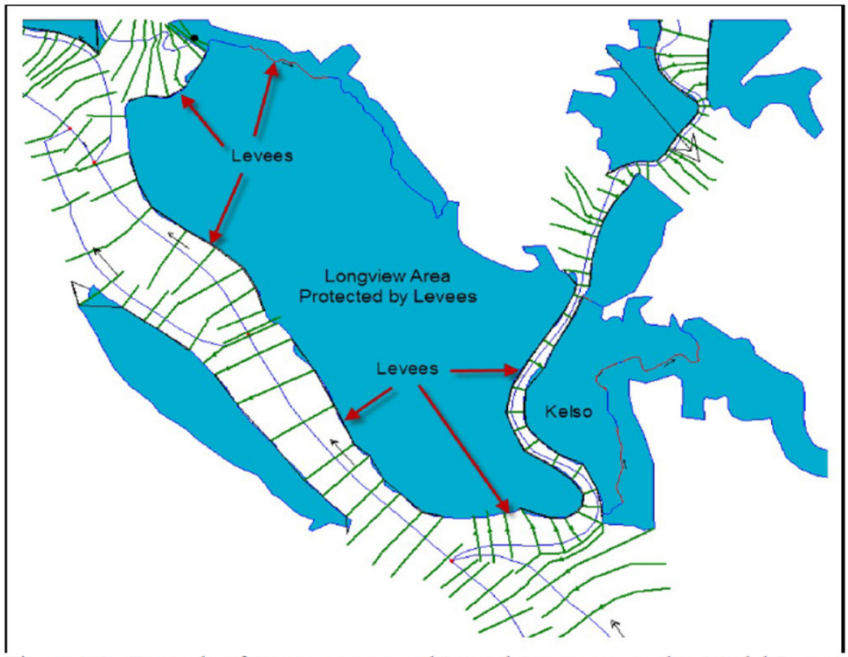

Figure 3-8. Example of Storage Areas and Lateral Structures used to Model Protected Areas

60

Kalibracija

Table 3-5. Manning's n Value Ranges for Main Channels and Overbank Areas

River Name	Main Channel Manning's n Coefficient	Overbank Manning's n Coefficient
Columbia River	0.028 - 0.035	0.05 - 0.10
Willamette River	0.03 - 0.039	0.05 - 0.15
Cowlitz River	0.025 - 0.031	0.05 - 0.10
Lewis River	0.032	0.05 - 0.10
All Other Channels	0.03	0.05 - 0.15

61

Table 3-6. Summary of Model Calibration Results

Location	Flood Event	Computed Peak Stage NAVD (feet)	Observed Peak Stage NAVD (feet)	Stage Difference (feet)	Time Difference (hours)
Columbia River @ Bonneville	1996	37.4	38.3	-0.9	0.0
	1997	37.8	38.0	-0.2	-1.0
	2008	32.2	32.4	-0.2	+1.0
Columbia River @ Vancouver	2008	20.3	20.1	+0.2	+1.0
Columbia River @ Saint Helens	2008	17.5	17.6	-0.1	-1.0
Columbia River @ Longview	2008	14.5	15.7	-1.2	-0.75
Columbia River @ Beaver Army Terminal	1996	17.3	16.4	+0.9	0.0
	1997	15.4	15.0	+0.4	0.0
	2008	13.0	13.3	-0.3	0.0
Columbia River @ Astoria	1996	11.8	12.1	-0.3	0.0
	1997	11.9	12.1	-0.2	-1.0
	2008	11.1	11.4	-0.3	+1.0
Willamette River Below Falls	1996	46.2	*49.2	-3.0	N/A
	1997	39.0	40.0	-1.0	+1.0
	2008	30.7	29.6	+1.1	-3.0
Willamette Reiver @ Portland	1996	33.0	32.7	+0.3	-1.0
	1997	28.3	28.0	+0.3	+3.0
	2008	19.9	19.6	+0.3	-1.0
Cowlitz River @ Castle Rock	1996	55.8	55.9	-0.1	-2.0
	1997	46.6	47.0	-0.4	-1.0
	2008	54.7	54.6	+.1	+0.75
Cowlitz River @ Lexington	2008	37.8	37.8	0.0	-1.0
Cowlitz River @ Ostrander	2008	30.6	30.6	0.0	+1.0
Cowlitz River @ Gearhart	2008	17.9	18.0	-0.1	0.75

*Note: Data value estimated from high water marks. This could actually be the energy gradeline instead of the true average water surface elevation.

62

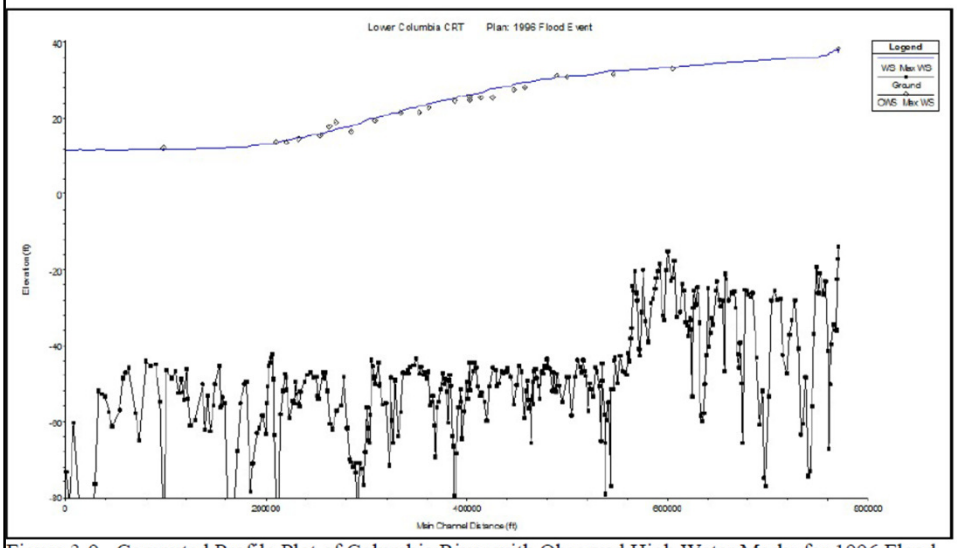

Figure 3-9. Computed Profile Plot of Columbia River with Observed High Water Marks for 1996 Flood

63

Verifikacija

Table 3-7. Summary of Model Verification Results

Location	Flood Event	Computed Peak Stage NAVD (feet)	Observed Peak Stage NAVD (feet)	Stage Difference (feet)	Time Difference (hours)
Columbia River @ Bonneville	2006	31.1	31.1	0.0	-2.0
	2010	31.2	31.9	-0.7	+1.0
Columbia River @ Vancouver	2006	20.1	20.4	-0.3	-4.0
	2010	19.8	20.0	-0.2	-2.0
Columbia River @ Saint Helens	2006	17.9	18.3	-0.4	-1.0
	2010	16.9	17.4	-0.5	0.0
Columbia River @ Longview	2006	14.9	15.5	-0.6	0.0
	2010	13.7	14.2	-0.5	0.0
Columbia River @ Beaver Army Terminal	2006	14.0	14.2	-0.2	0.0
	2010	12.0	12.0	0.0	0.0
Columbia River @ Astoria	2006	12.4	12.5	-0.1	0.0
	2010	10.3	10.8	-0.5	0.0
Willamette River Below Falls	2006	32.1	31.8	+0.3	+2.0
	2010	25.0	24.5	+0.5	+2.0
Willamette River @ Portland	2006	20.8	20.4	+0.4	+3.0
	2010	19.4	19.5	-0.1	-2.0
Cowlitz River @ Castle Rock	2006	46.6	45.7	+0.9	-1.0
	2010	37.8	38.0	-0.2	0.0

64

HEC-RAS 2D stacionarno

Primjer 1: Uspor (*backwater*) – usporedba sa ručnim izračunom i 1D modelom

Table 3-2. Specifications for the San Joaquin Canal Test Case

Parameter	Value
Bottom width, b (feet)	40
Side slopes, z	1.5:1 H:V
Bed slope, S	0.00005
Roughness, n	0.012
Flow rate, Q cfs	1,700 to 0.0
Downstream Gated Structure, Gate Openings (feet)	2.6 to 0.0
Downstream Boundary Condition, WS (feet)	219.8

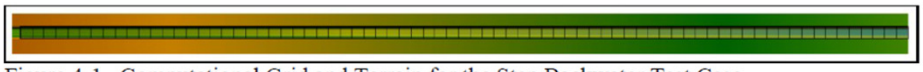

Figure 4-1. Computational Grid and Terrain for the Step Backwater Test Case

Table 4-2. Model Setup Parameters for the Step Backwater Test Case

Parameter	Value
Governing equations	SWE
Manning's n roughness coefficient ($s/m^{1/3}$)	0.025
Turbulence	Off
Time step (second)	2
Simulation duration (hour)	1
Implicit weighting factor	1
Water surface tolerance (meter)	0.0001
Volume tolerance (meter)	0.0001

65

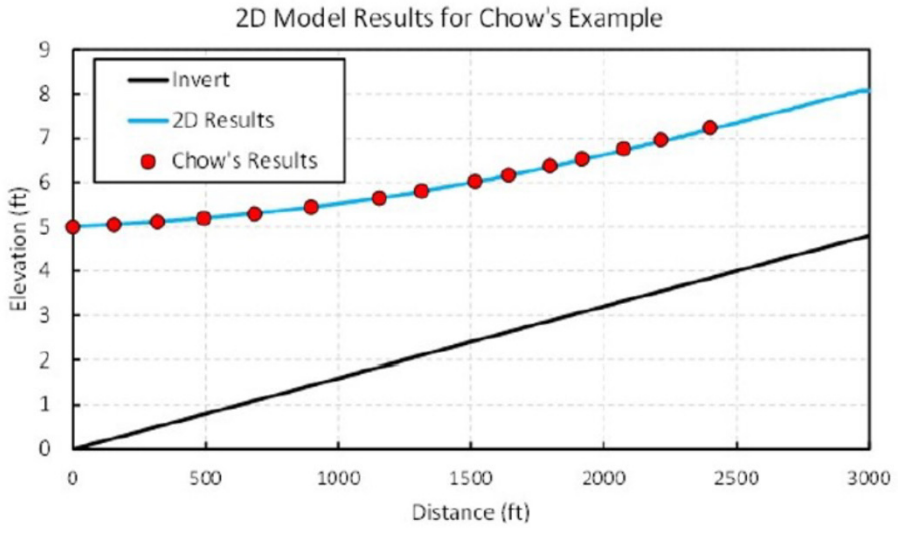

Figure 4-2. Velocity Plot with Profile Lines at Locations of Velocity Measurements

66

HEC-RAS 2D stacionarno

Primjer 2: Tečenje preko izbočine – tranzicija režima

$$z_b = \begin{cases} 0, & \text{for } x < 8 \\ 0.2 - 0.05(x-10)^2, & \text{for } 8 \le x < 12 \\ 0, & \text{for } 12 \le x \end{cases}$$

Table 2-2. Specifications for the One-Dimensional Transcritical Flow over a Bump without Friction Test Case

Parameter	Value
Bottom width, b (meter)	0.3
Side slopes, z	0.0
Bed slope, S	0.0
Roughness, frictionless, n	0.0001
Flow rate, Q cms (cubic meter per second)	0.054
Downstream Boundary Condition, WS (meter)	0.33

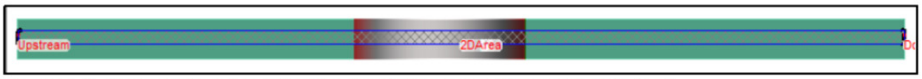

Figure 4-5. Computational Grid for the Two-Dimensional Bump Test Dataset

Table 4-6. Model Setup Parameters for the Two-Dimensional Bump Test Case

Parameter	Value
Manning's roughness coefficient ($s/m^{1/3}$)	0.00001
Grid resolution (meter)	0.05
Governing equations	SWE
Implicit weighting factor	1.0
Water Surface Tolerance (meter)	1×10^{-3}
Volume Tolerance	1×10^{-3}
Mixing coefficient	0.0
Upstream discharge (m^3/s)	0.054
Downstream water level (meter)	0.33
Initial water depth (meter)	0.33
Simulation duration (minutes)	5

67

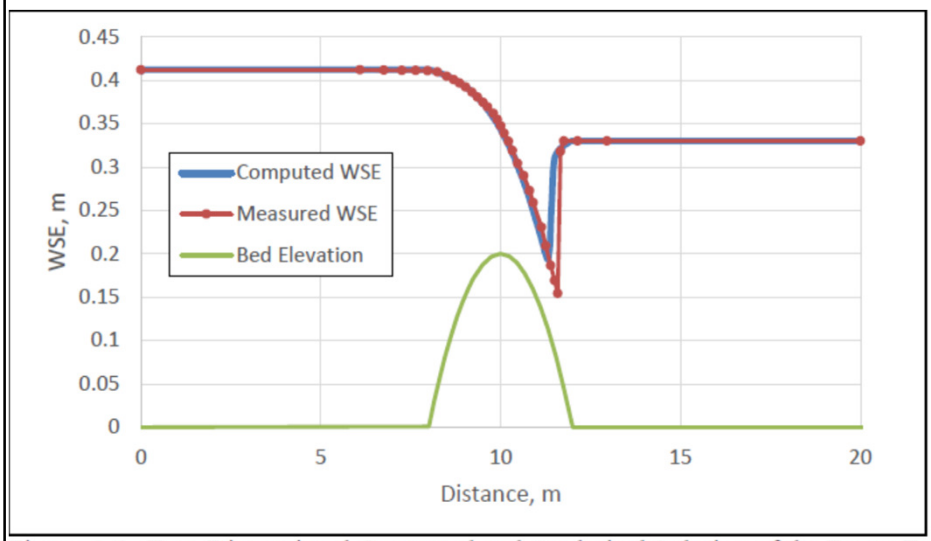

Figure 4-6. Two-Dimensional Computed and Analytical Solution of the Bump Test

68

HEC-RAS 2D stacionarno

Primjer 3: Tečenje u kanalu pravokutnog presjeka s naglim proširenjem (usporedba s laboratorijskim eksperimentom)

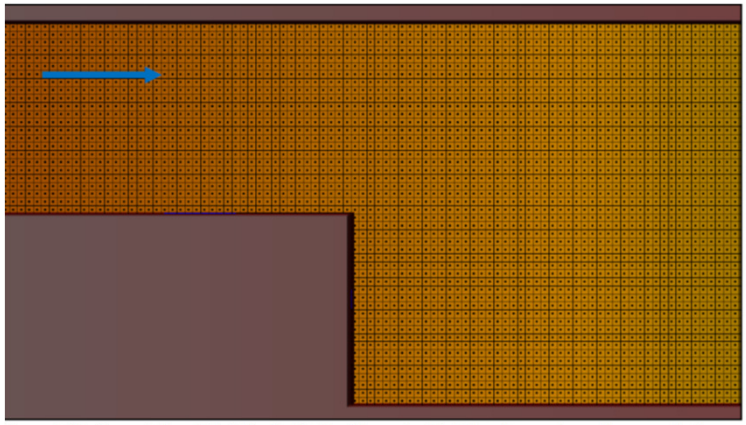

Figure 4-33. Computational Mesh for the Sudden Expansion Test Case (zoomed near the expansion)

69

Table 4-23. Specifications of the Sudden Expansion Flume Experiment

Item	Value
Bottom width, B (meter)	0.6 (upstream); 1.2 (downstream)
Bed slope	$S_0 \approx 0$
Channel roughness, n	0.015 (bottom); 0.008 (wall, glass)
Upstream boundary condition, flow, Q (cms)	0.01815 and 0.03854
Downstream boundary condition, stage, h (meter)	0.11

Table 4-24. Model Specifications for the Sudden Expansion Test Case

Item	Value
Mesh cell size (meter)	0.025
Manning's n	0.015 and 0.008
Time step	0.05 s ($Cr_{max} \approx 1$), for Q=0.01815 cms 0.033 s ($Cr_{max} \approx 1$), for Q=0.03854 cms
Theta	1.0
Eddy viscosity coefficient	1.4
Equation set	Full momentum

70

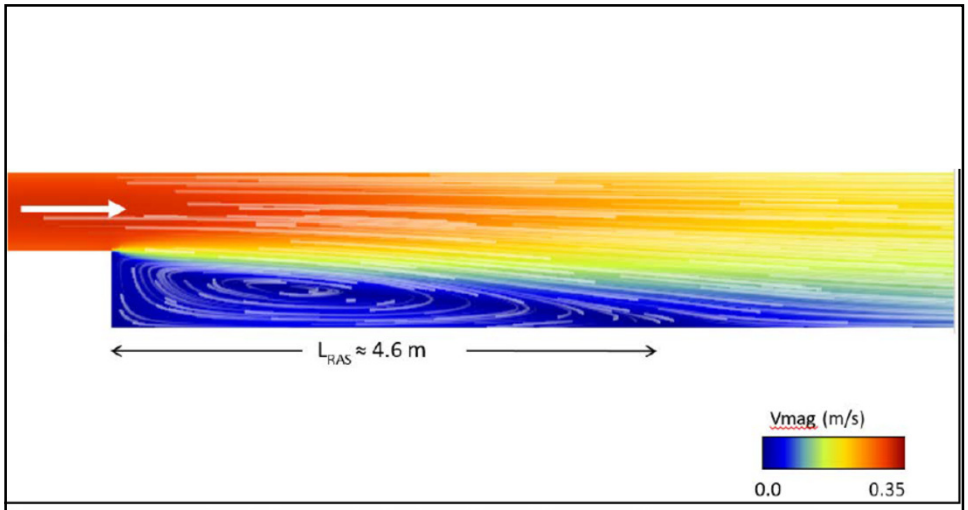

Figure 4-34. Computed Velocity Magnitude Plot with Particle Traces (for Q=0.01815 cms), the Blue Shaded Eddy Zone is Clearly Evident Downstream of the Expansion

71

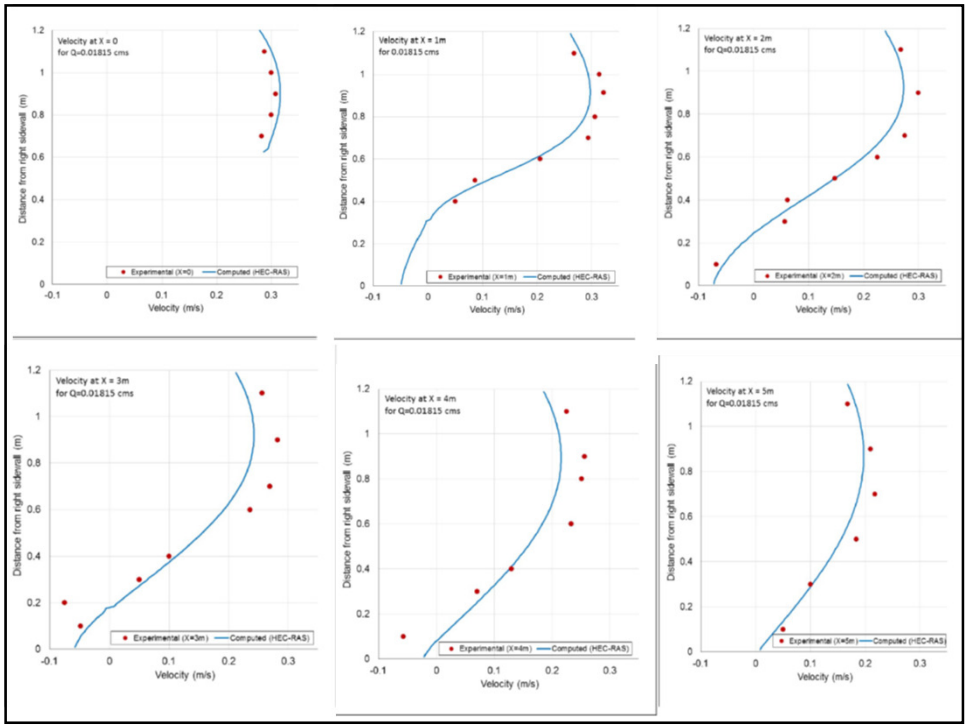

72

HEC-RAS 2D stacionarno

Primjer 4: Tečenje u kanalu pravokutnog presjeka sa 180o zavojem
(usporedba s laboratorijskim eksperimentom)

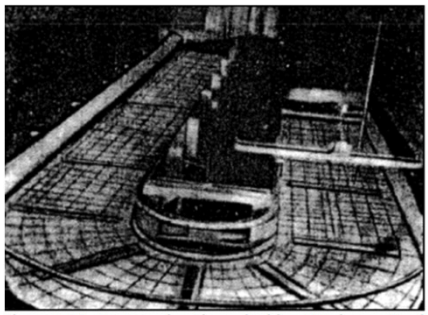

Figure 4-53. Rectangular Channel with a 180-degree Bend (Rozovskii, 1957)

Table 4-27. Specifications of the 180-degree Bend Flume Experiment

Item	Value
Bottom width (rectangular), B (meter)	0.8
Bed slope, S_0	0
Channel roughness (smooth), n	0.01
Bend mean radius-to-width ratio (tight bend)	1.0
Upstream boundary condition, low	Q = 0.0123 cms (subcritical flow) and F=0.11
Downstream boundary condition, stage, h (meter)	0.057

73

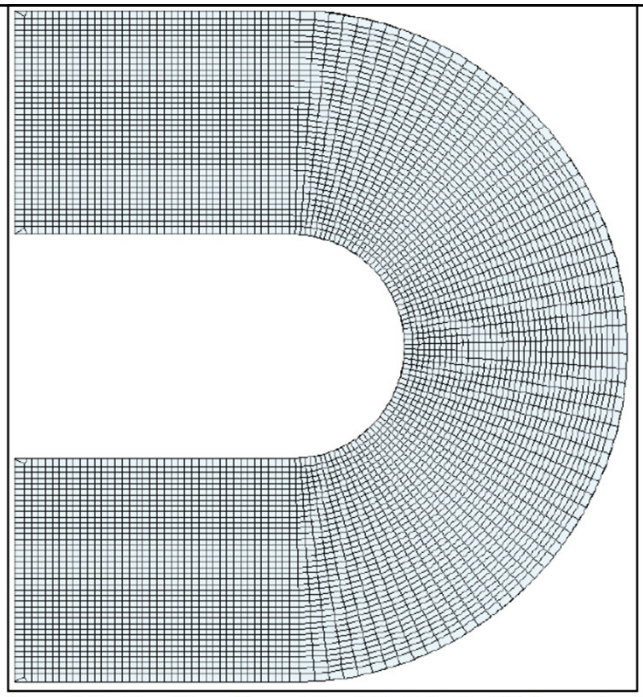

Figure 4-54. Curvilinear Computational Mesh for the 180-degree Bend Test Case

74

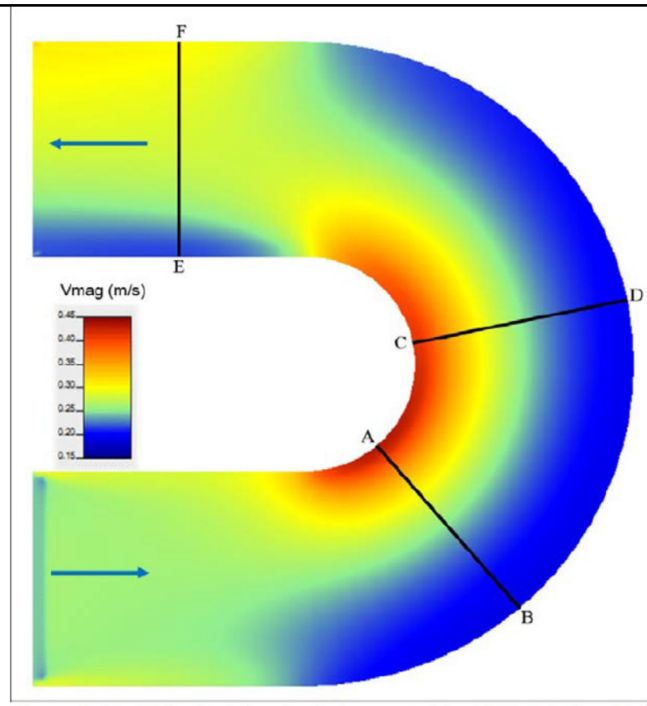

Figure 4-55. Velocity Magnitude (computed by HEC-RAS), with I

75

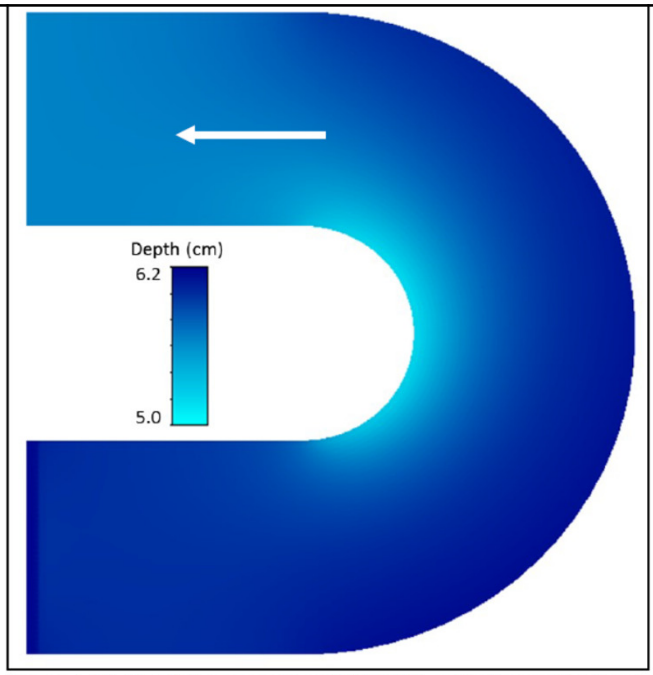

Figure 4-59. Depth (computed by HEC-RAS), with Deeper Depths along Outside of Bend (super-elevation)

76

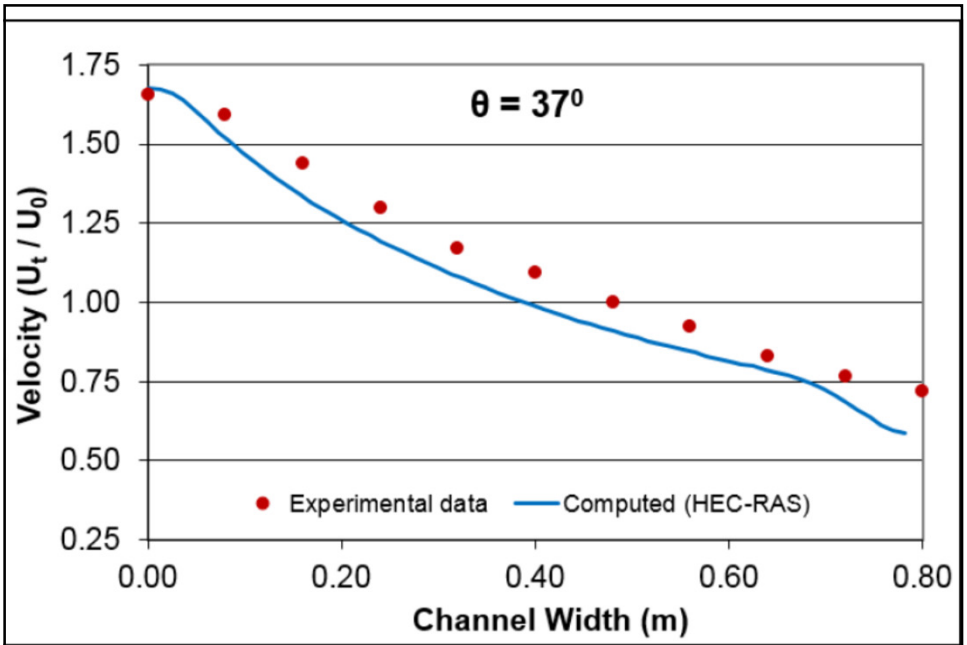

Figure 4-56. Velocity Profile (computed and experimental), at Section A-B in Figure 4-55 (with entrance velocity $U_0 = 0.265$ m/s)

77

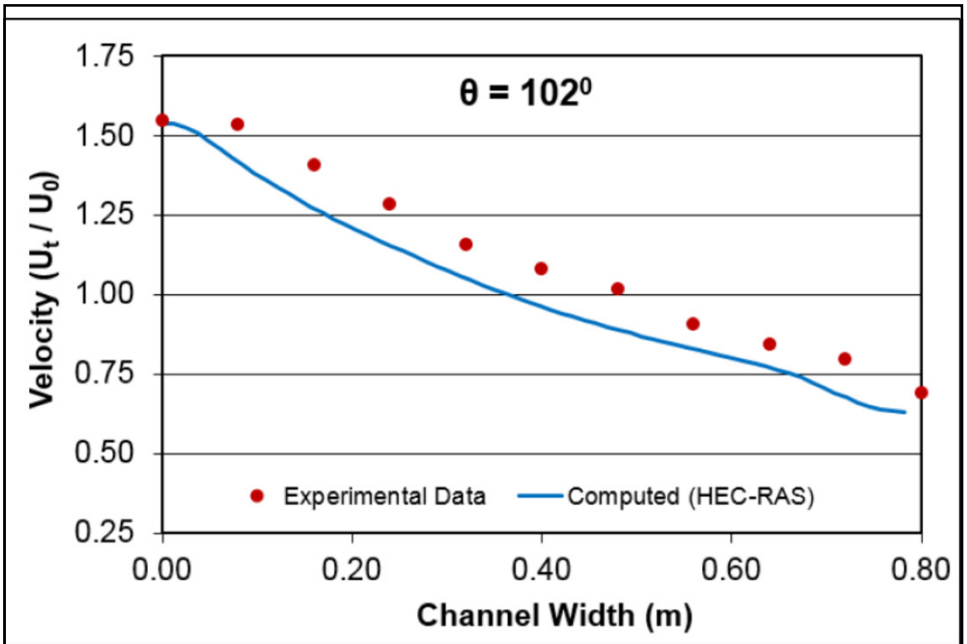

Figure 4-57. Velocity Profile (computed and experimental), at Section C-D in Figure 4-55 (with entrance velocity $U_0 = 0.265$ m/s)

78

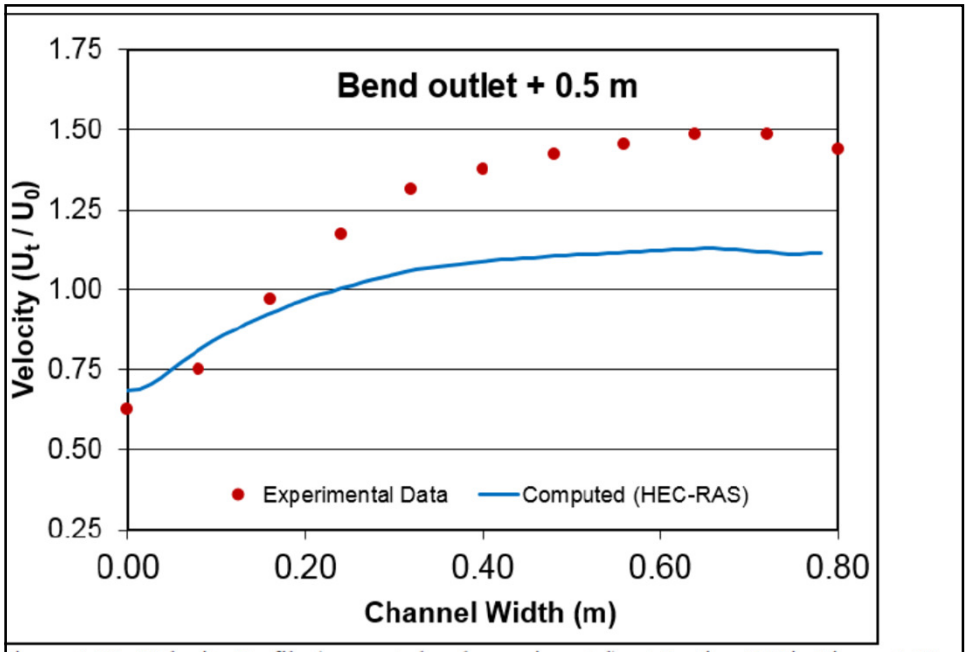

Figure 4-58. Velocity Profile (computed and experimental), at Section E-F in Figure 4-55 (with entrance velocity U_0=0.265 m/s)

79

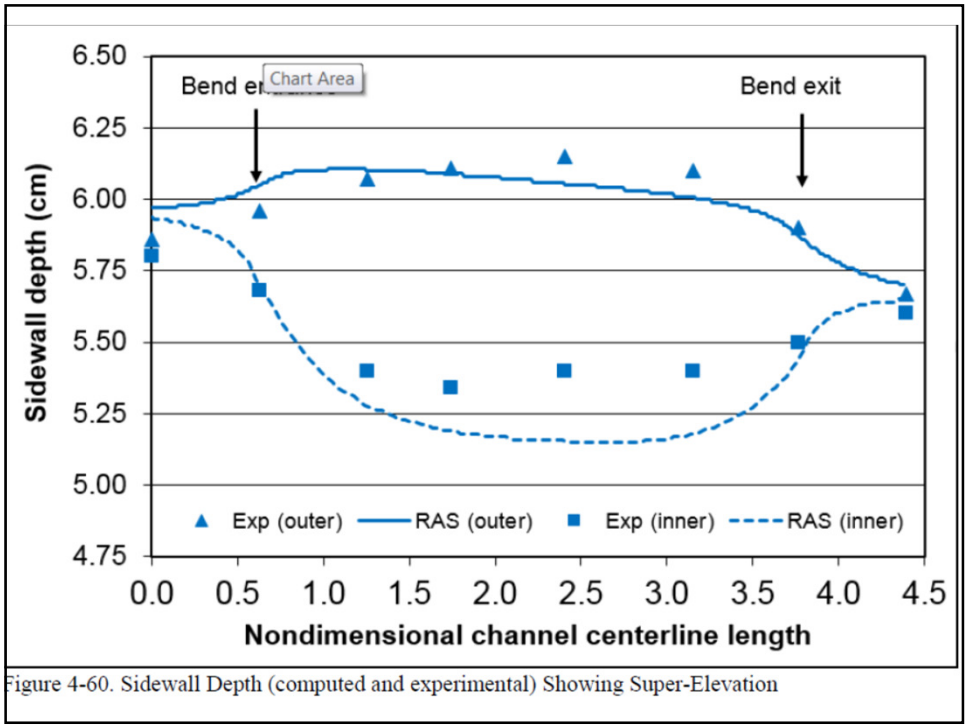

Figure 4-60. Sidewall Depth (computed and experimental) Showing Super-Elevation

80

HEC-RAS 2D stacionarno

Primjer 5: Tečenje oko pera
(usporedba s laboratorijskim eksperimentom)

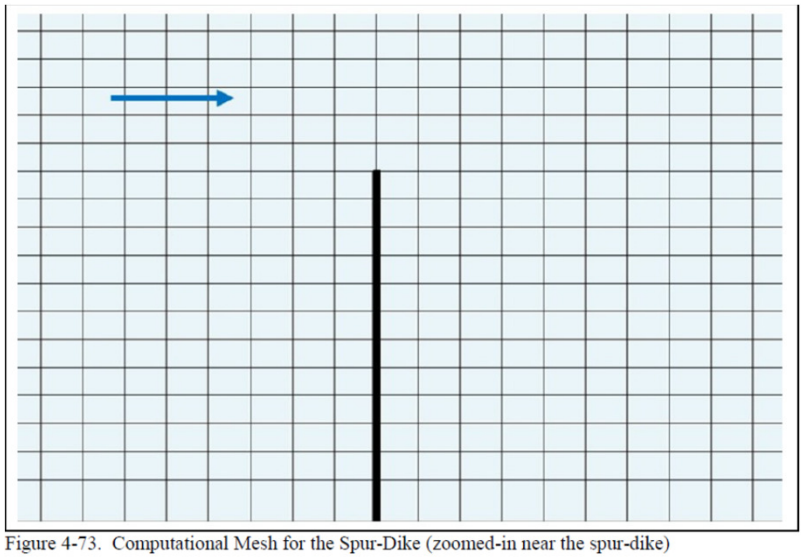

Figure 4-73. Computational Mesh for the Spur-Dike (zoomed-in near the spur-dike)

81

Table 4-34. Specifications of the Spur-Dike Experiment

Item	Value
Bottom width, B (meter)	0.915
Spur (or groin), b (mm)	150 mm long x 3 mm thick
Bed slope, S_0	≈ 0
Channel roughness, n	0.01 (smooth)
Upstream boundary condition, flow, Q (cms)	0.043 with $U_0 \approx 0.252$ m/s
Downstream Boundary, stage, h (meter)	0.189

Table 4-35. Model Specifications for the Spur-Dike Test Case

Item	Value
Mesh cell size (meter)	0.015 x 0.015 m
Manning's n	0.01
Time step (second)	0.01 ($Cr_{max} \approx 1$)
Theta	1.0
Eddy viscosity coefficient	2.0
Equation set	Full momentum

82

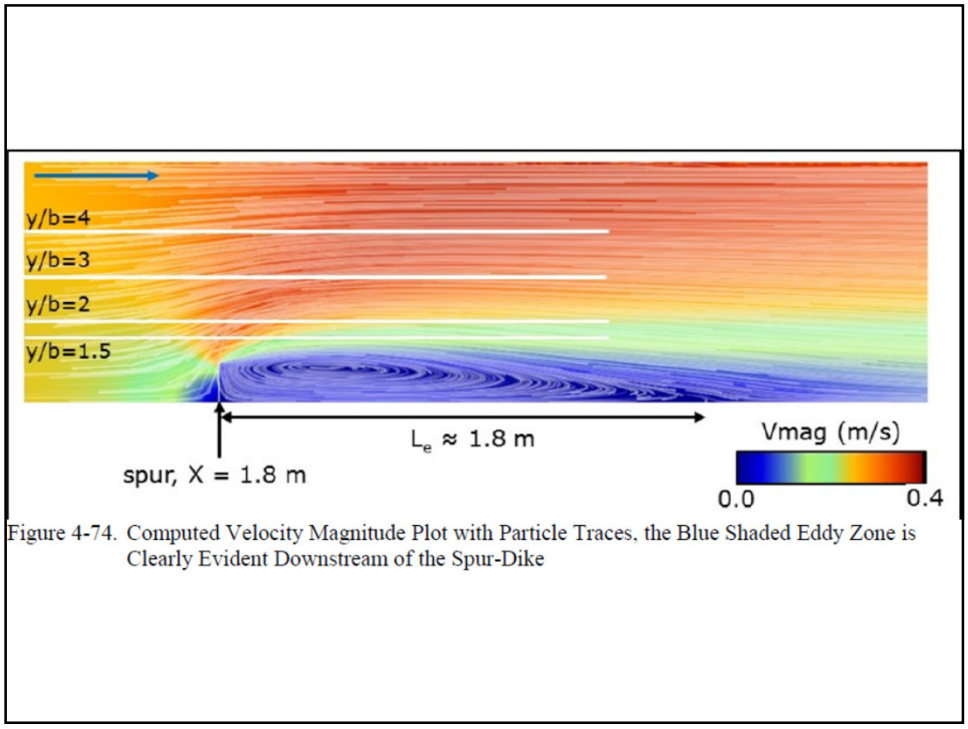

Figure 4-74. Computed Velocity Magnitude Plot with Particle Traces, the Blue Shaded Eddy Zone is Clearly Evident Downstream of the Spur-Dike

83

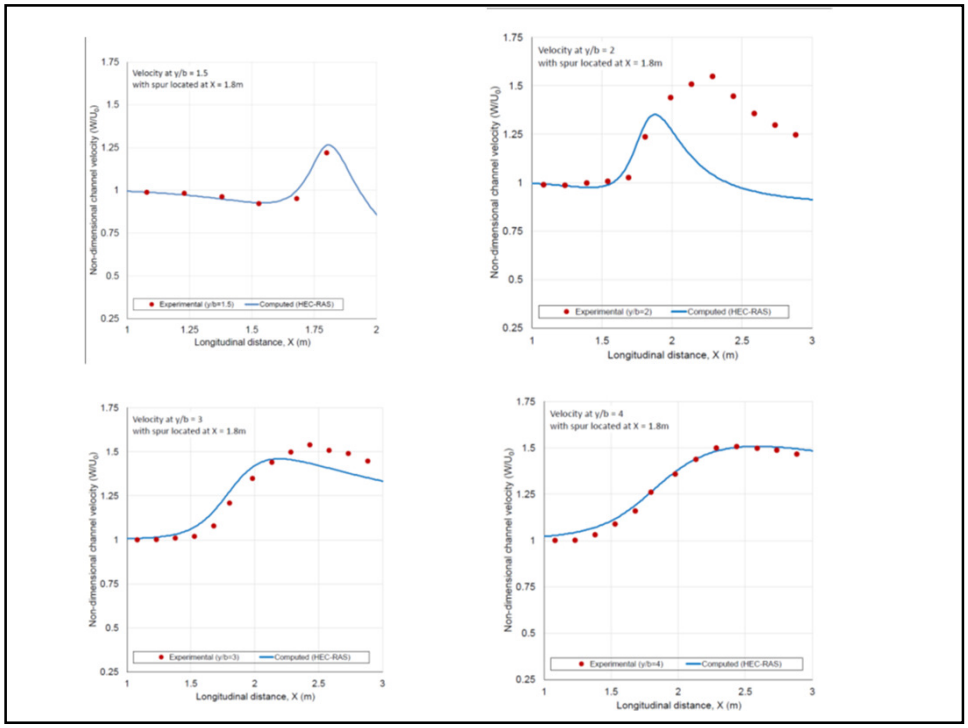

84

HEC-RAS 2D nestacionarno

Primjer 1: Propagacija vodnog vala na ravnom dnu
(usporedba s analitičkim rješenjem)

$$\frac{\partial U}{\partial t} + \frac{\partial (hU)}{\partial x} = 0$$

$$\frac{\partial U}{\partial t} + U\frac{\partial U}{\partial x} = -g\frac{\partial \eta}{\partial x} - \frac{\tau_b}{\rho}$$

$$h = \left\{\frac{7}{3}[C - n^2U^3(x - Ut)]\right\}^{3/7}$$

Table 4-7. Convergence Criteria Analyzed after each Outer Loop Iteration

Parameter	Value
Manning's roughness coefficient, n (s/m$^{1/3}$)	0.01
Current velocity u (m/s)	1
Grid resolution (meter)	25
Initial water surface elevation (meter)	0
Governing equations	SWE, DWE
Time step (seconds)	10
Implicit weighting factor	1 (default)
Water Surface Tolerance (meter)	0.001 (default)
Volume Tolerance (meter)	0.001 (default)

85

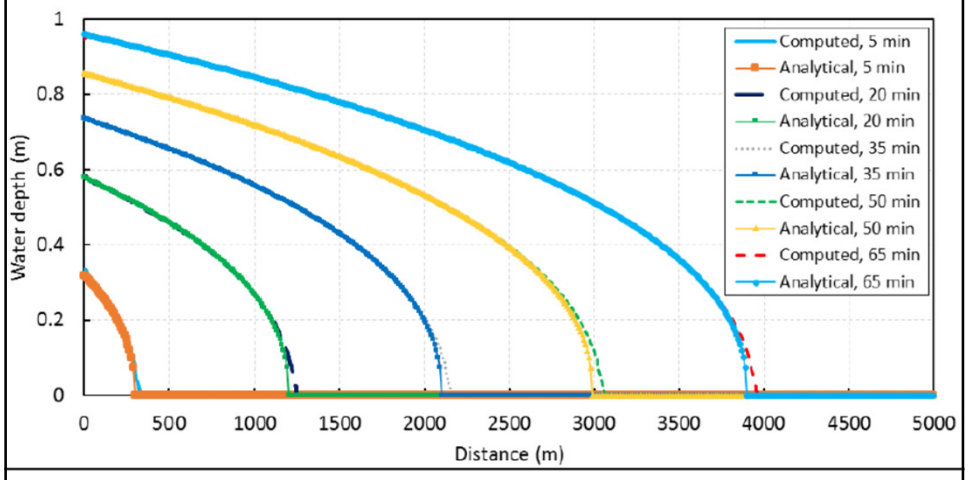

86

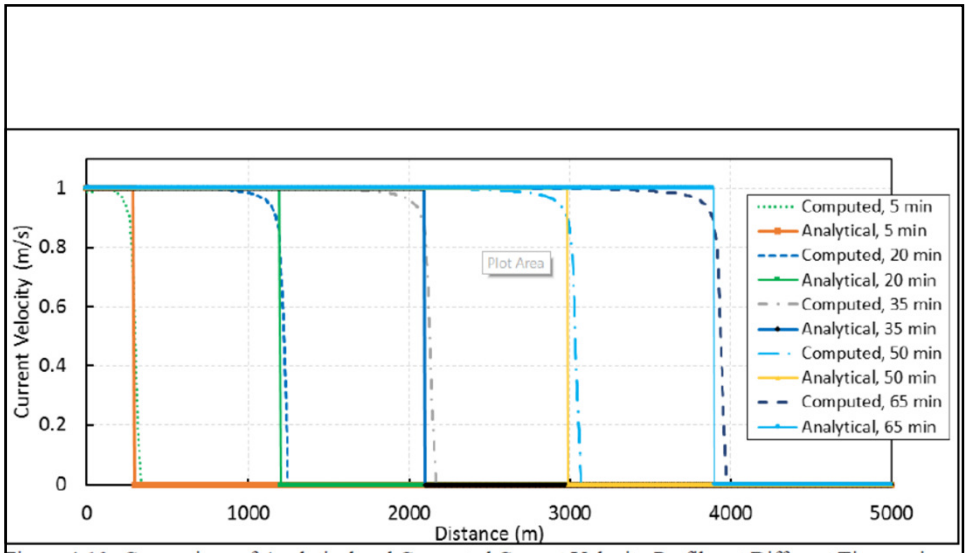

Figure 4-10. Comparison of Analytical and Computed Current Velocity Profiles at Different Times using the HEC-RAS Shallow Wave Equation (SWE) Solver

87

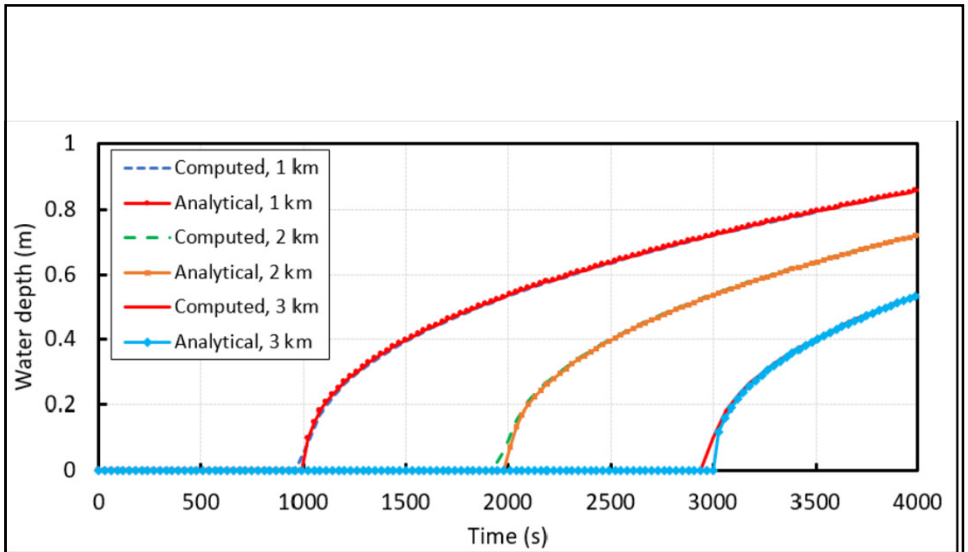

Figure 4-12. Comparison of Analytical and Computed Water Depth Time-series at Three Stations using the HEC-RAS Shallow Water Equation (SWE) Solver

88

HEC-RAS 2D nestacionarno

Primjer 2: Pucanje brane na ravnom dnu (usporedba s analitičkim rješenjem)

$$\frac{\partial h}{\partial t} + \frac{\partial q}{\partial x} = 0$$

$$\frac{\partial q}{\partial t} + \frac{\partial}{\partial x}\left(\frac{q^2}{h}\right) + \frac{g}{2}\frac{\partial h^2}{\partial x} = 0$$

$$h = \begin{cases} h_L & \text{for } x \le x_l \\ h_r & \text{for } x_l < x < x_r \\ h_* & \text{for } x_r \le x < x_* \\ h_R & \text{for } x \ge x_* \end{cases} \qquad U = \begin{cases} 0 & \text{for } x \le x_l \\ U_r & \text{for } x_l < x < x_r \\ U_* & \text{for } x_r \le x < x_* \\ 0 & \text{for } x \ge x_* \end{cases}$$

$$h(x, t=0) = \begin{cases} h_L & \text{for } x < x_0 \\ h_R & \text{for } x_0 \ge x \end{cases}$$

$$U(x, t=0) = \frac{q}{h} = 0$$

$$h_r = \frac{1}{g}\left(\frac{2}{3}\sqrt{gh_L} - \frac{x - x_0}{3t}\right)^2$$

$$U_r = \frac{2}{3}\left(\sqrt{gh_L} - \frac{x - x_0}{t}\right)$$

h_* = positive wave water depth [L]

U_* = positive wave current velocity [L]

$$x_r = x_0 + t\left(2\sqrt{gh_L} - 3\sqrt{gh_*}\right)$$

$$x_l = x_0 - t\sqrt{gh_L}$$

$$x_* = x_0 + t\sqrt{gh_R}\sqrt{\frac{h_*}{2h_R}\left(1 + \frac{h_*}{h_R}\right)}$$

Table 4-8. Model Setup Parameters for the Dam Break Test Cases

Parameter	Value
Manning's roughness coefficient (s/m$^{1/3}$)	1x10^{-6}
Grid resolution (meter)	1
Initial left water depth (meter)	10
Initial right water depth (meter)	0, 5
Initial current velocity (meter per second)	0
Governing equations	SWE
Time step (second)	0.05
Implicit weighting factor	0.6
Water Surface Tolerance (meter)	1 x 10^{-5}
Volume Tolerance (meter)	1 x 10^{-5}
Mixing coefficient	0.0
Simulation duration (second)	60

89

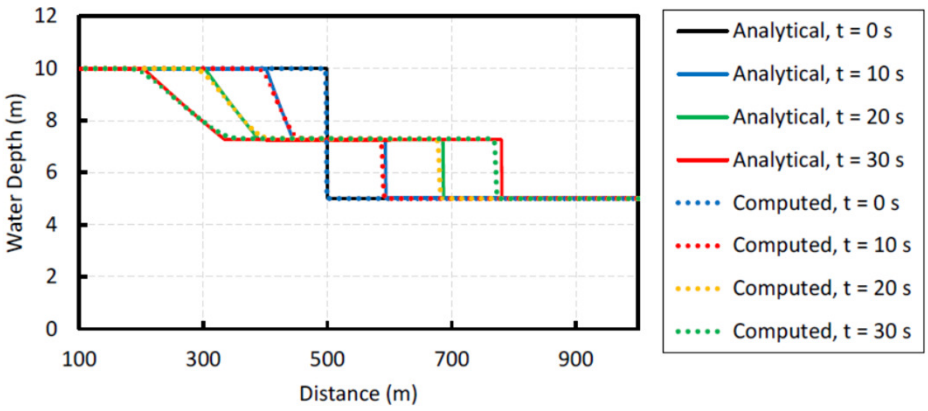

Figure 4-13. Computed and Analytical Water Depths for the Idealized Dam Break Test Case

90

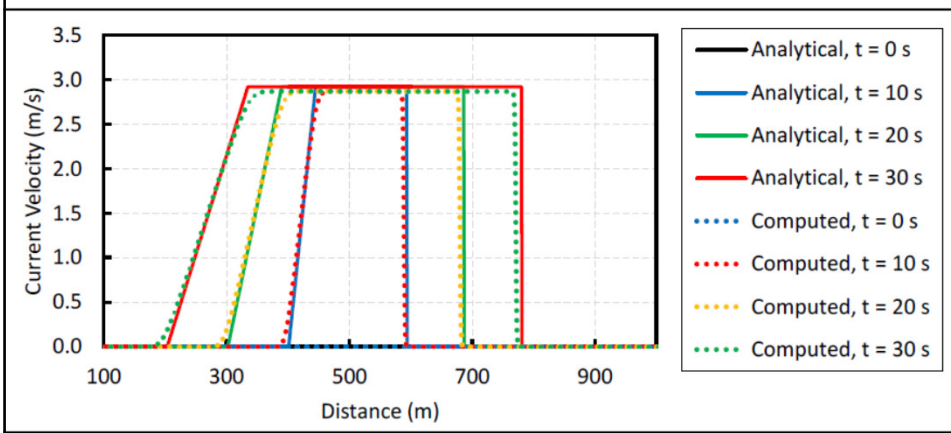

Figure 4-14. Computed and Analytical Current Velocities for the Idealized Dam Break Test Case

91

HEC-RAS 2D nestacionarno

Primjer 3: Udar vala velike valne duljine (tsunami) u obalu pod nagibom (usporedba s analitičkim rješenjem)

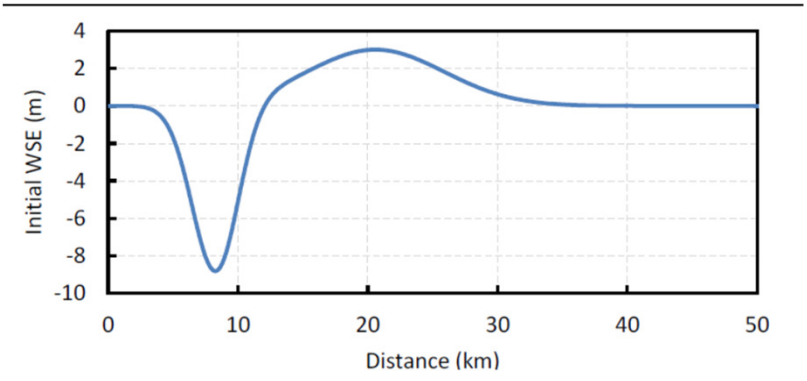

92

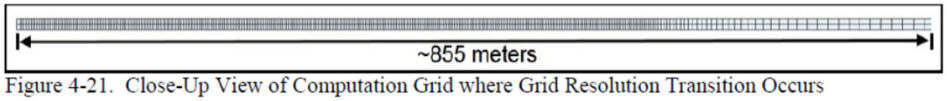

Figure 4-21. Close-Up View of Computation Grid where Grid Resolution Transition Occurs

Table 4-14. Model Setup Parameters for the Long-Wave Run-Up on a Planar Slope Test Case

Parameter	Value
Manning's roughness coefficient ($s/m^{1/3}$)	0.0000001
Grid resolution (meter)	5 (constant)
Governing equations	SWE
Time step (second)	0.1
Implicit weighting factor	1.0
Water Surface Tolerance (meter)	1×10^{-5}
Volume Tolerance(meter)	1×10^{-5}
Mixing coefficient	0.0
Simulation duration (second)	360

93

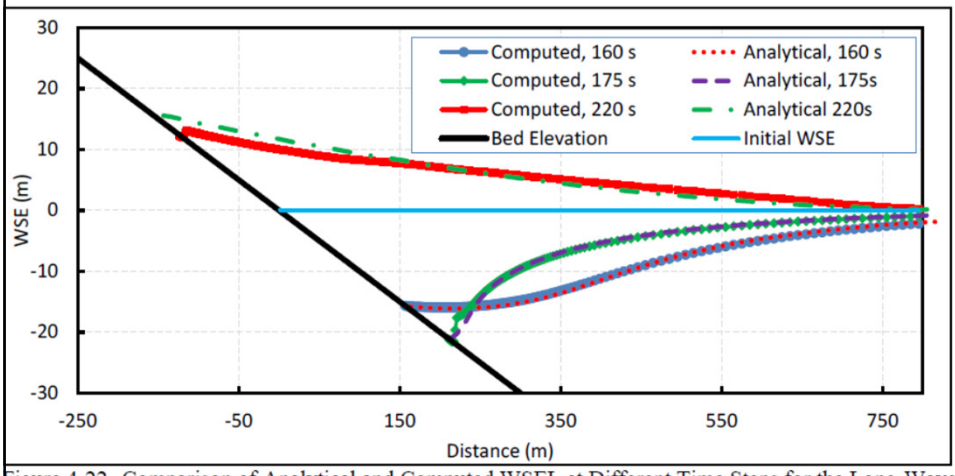

Figure 4-22. Comparison of Analytical and Computed WSEL at Different Time Steps for the Long-Wave Run-Up Test Case

94

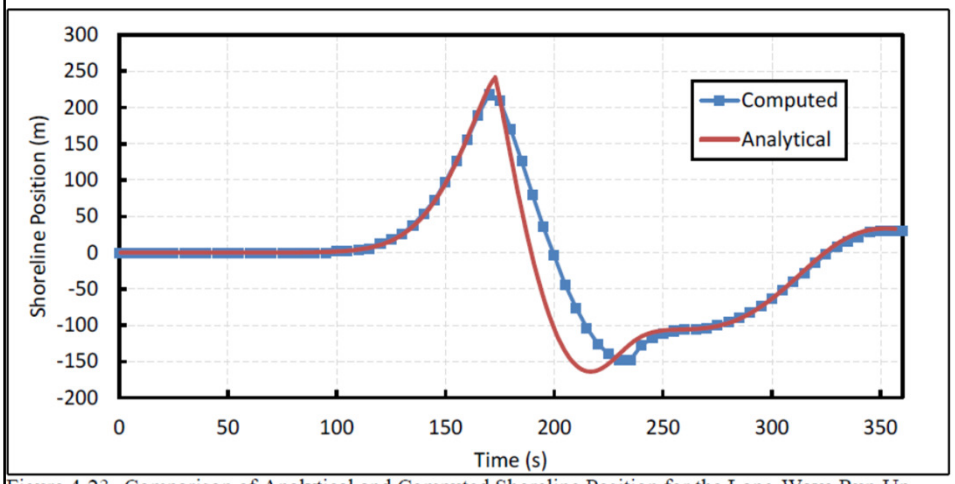

Figure 4-23. Comparison of Analytical and Computed Shoreline Position for the Long-Wave Run-Up Test Case

95

HEC-RAS 2D nestacionarno

Primjer 4: Površinsko otjecanje sa sliva
(usporedba s laboratorijskim eksperimentom)

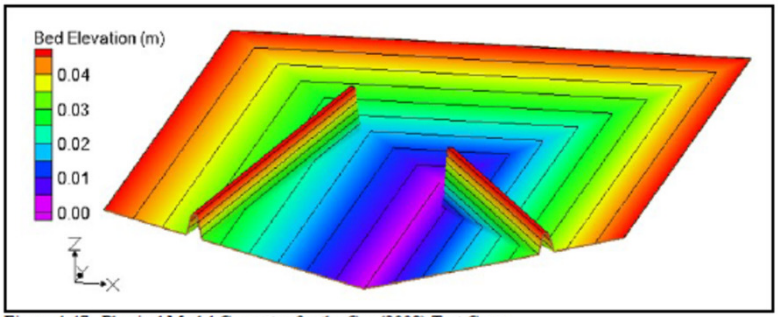

Figure 4-47. Physical Model Geometry for the Cea (2008) Test Cases

96

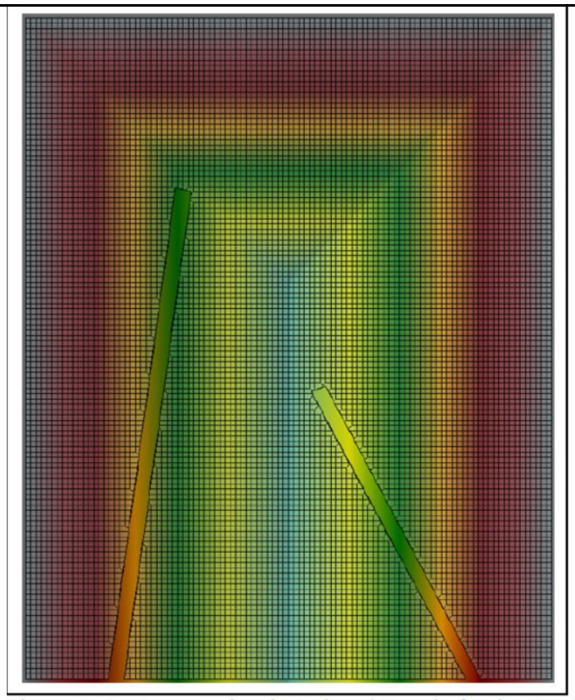

Figure 4-48. Computational Mesh and Terrain for the Cea (2008) Test Cases

97

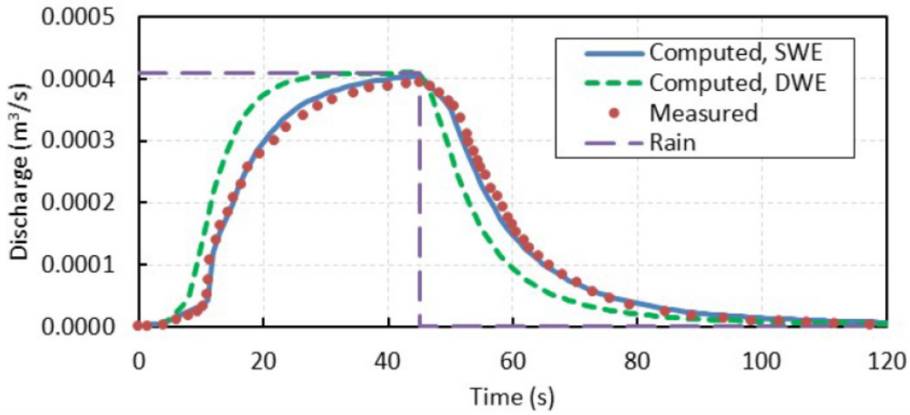

Figure 4-49. Comparison of Measured and Computed Discharge for Test Case C1 (Coe, 2008)

98

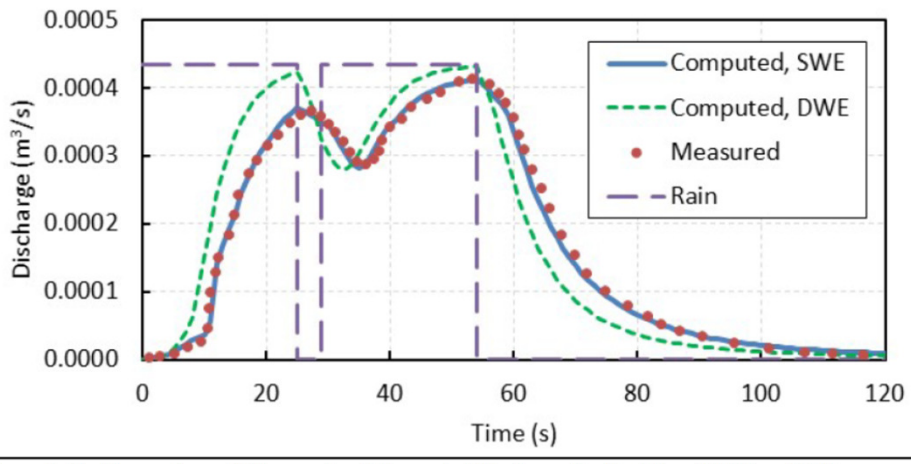

Figure 4-50. Comparison of Measured and Computed Discharge for Test Case 2B (Coe, 2008)

99

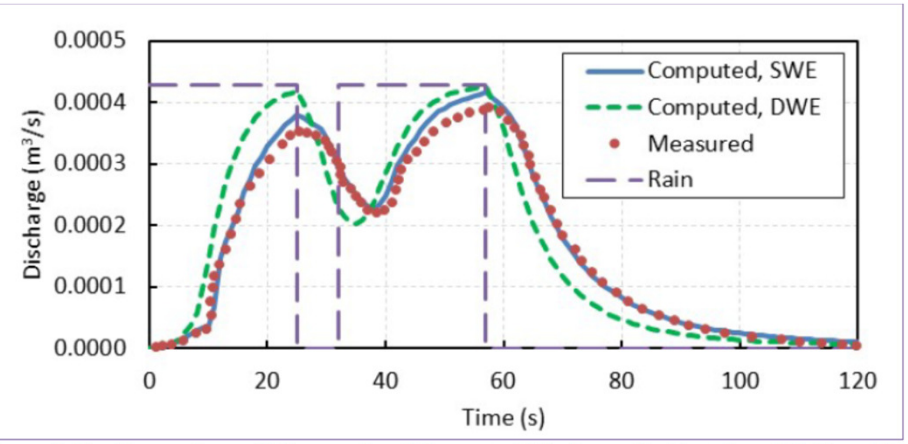

Figure 4-51. Comparison of Measured and Computed Discharge for Test Case 2C (Coe, 2008)

100

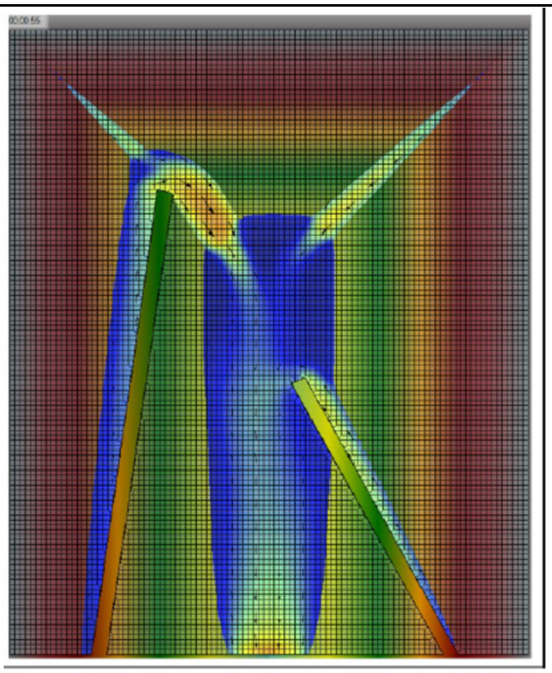

Figure 4-52. Example Current Velocity Field for Test Case 2C at 55 seconds

101

HEC-RAS 2D nestacionarno

Primjer 5: Pucanje brane Malpasset, Francuska
(usporedba s terenskim podacima)

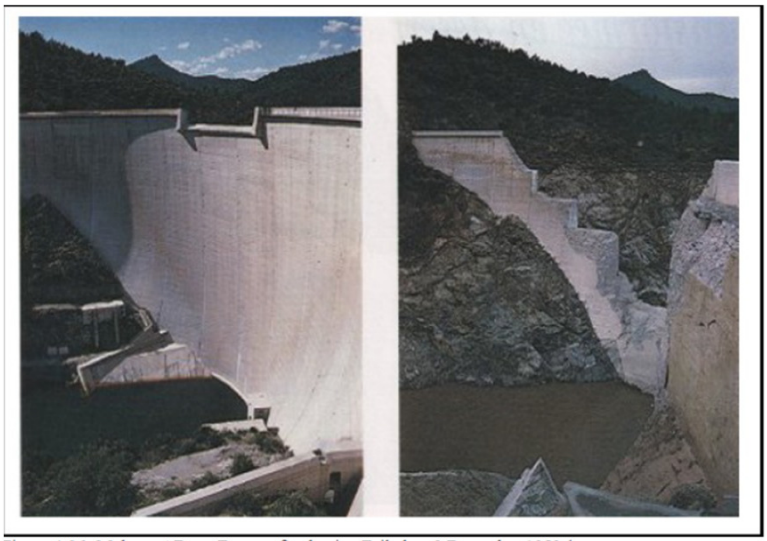

Figure 4-96. Malpasset Dam, France after having Failed on 2 December 1959 (source http://ecolo.org/documents/documents_in_french/malpasset/malpasset.htm)

102

Problem and Data Description

The Malpasset Dam was located in a narrow gorge on the Reyran River about 7 km north of Fréjus on the South West Coast of France. The arch dam was 66.5-meters tall and 223-meters wide at the crest (Figure 4-96). The capacity of the reservoir behind the dam was 55 million m^3. Construction on the dam began in 1952 and was completed in 1954. The dam had an emergency spillway and a low flow gate near the bottom. The dam was only 6.7 meters wide at the base and 1.5 meters wide at the crest. Between 19 November and 2 December 1959, there was approximately 20 inches of rainfall in 24-hours, raising the water level to within twelve inches of the spillway. On 2 December 1959, at 18:00 hours the water release valves were opened with a discharge rate of 40 m^3/s. Unfortunately, this was not enough to empty the reservoir in time and at 21:14 hours, the dam failed, explosively releasing 48 million m^3 of water and flooding the towns of Malpasset, Bozon, and Frejus, France.

103

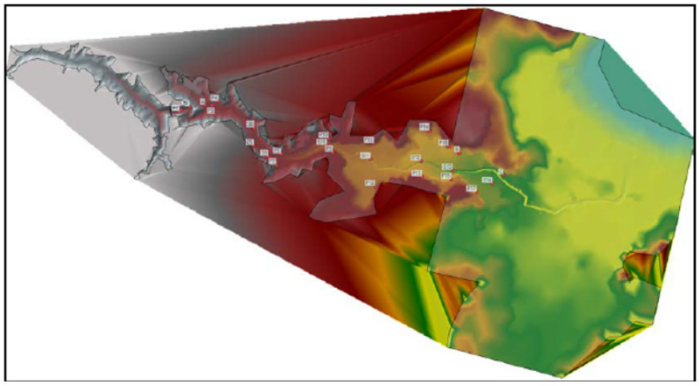

Figure 4-97 shows a map with the terrain and the location of measurement stations. The terrain was obtained from a previous existing mesh for the area from the study of Savant (2011). The terrain outside of the bounding polygon is not real since it is a result of spatial interpolations and therefore can be ignored. The terrain outside of the bounding polygon it is not used in the HEC-RAS model. The original terrain was digitized from an Institute Géographique national 1:20,000 map of Saint-Tropez n 3 from 1931. Stations A, B, and C (Figure 4-97) represent destroyed electric transformers which were used to estimate the flood wave arrival times. Stations beginning with a letter P (Figure 4-97) indicate maximum water level survey locations by the police after the event. Stations beginning with a letter S (Figure 4-97) indicate experimental measurement stations from a scaled physical model built at the Laboratoire National d'Hydraulique in 1964. The scale factor of the undistorted model was 1:400 (Soares Frazão, 2000).

104

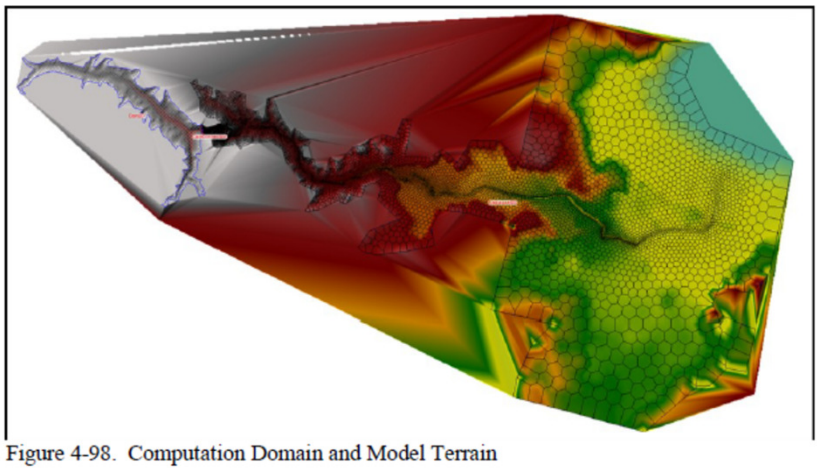

Figure 4-98. Computation Domain and Model Terrain

105

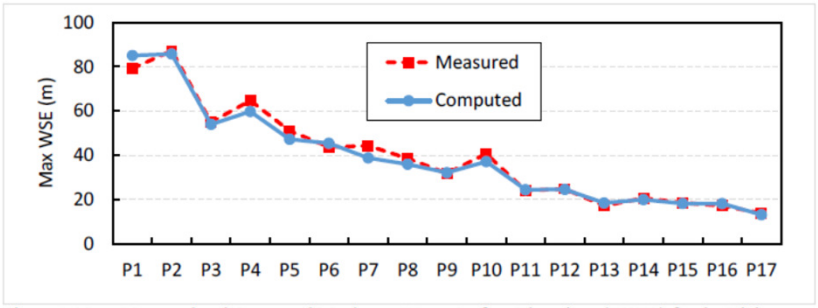

Figure 4-99. Measured and Computed Maximum Water Surface Elevations (WSEL) for the High-Water Marks Collected by the Police after the Malpasset Dam Break

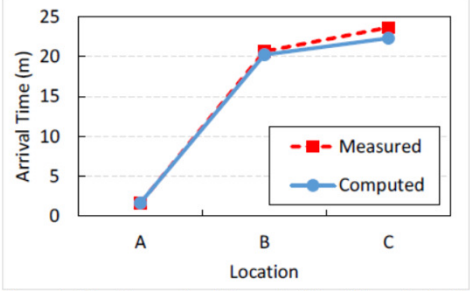

Figure 4-100. Measured and Computed Flood Wave Arrival Times for the Malpasset Dam Break at Three Locations where Electric Transformers were Damaged

106

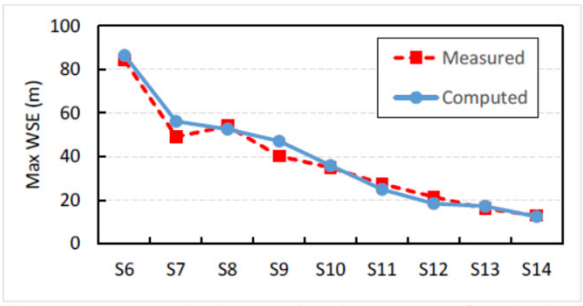

Figure 4-102. Measured and Computed Maximum Water Surface Elevations (WSEL) as Estimated by a Physical Model of the Malpasset Dam Break

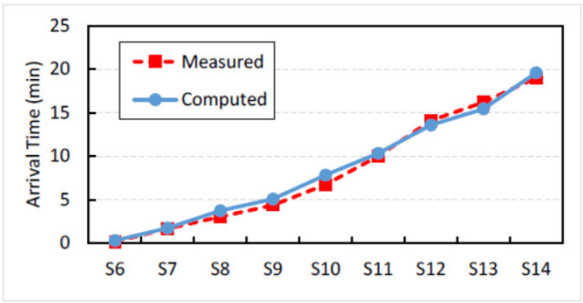

Figure 4-103. Measured and Computed Arrival Times (minutes) as Estimated by a Physical Model of the Malpasset Dam Break.

107

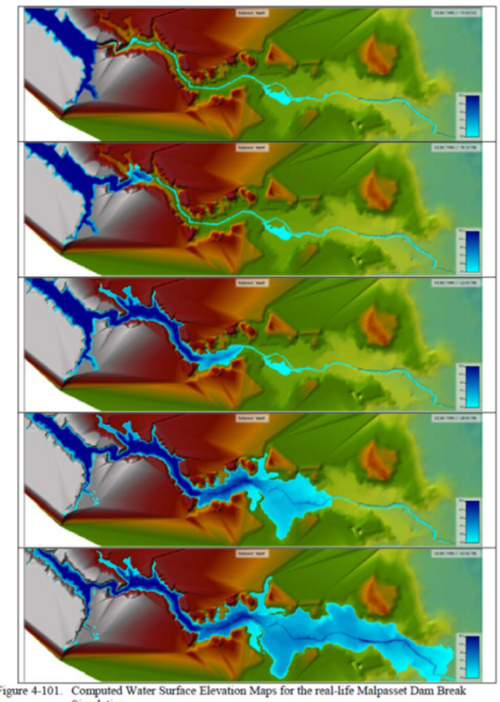

Figure 4-101. Computed Water Surface Elevation Maps for the real-life Malpasset Dam Break Simulation

108

HEC-RAS 2D nestacionarno

Primjer 6: Proboj nasipa na rijeci Mississipi
(usporedba s terenskim podacima)

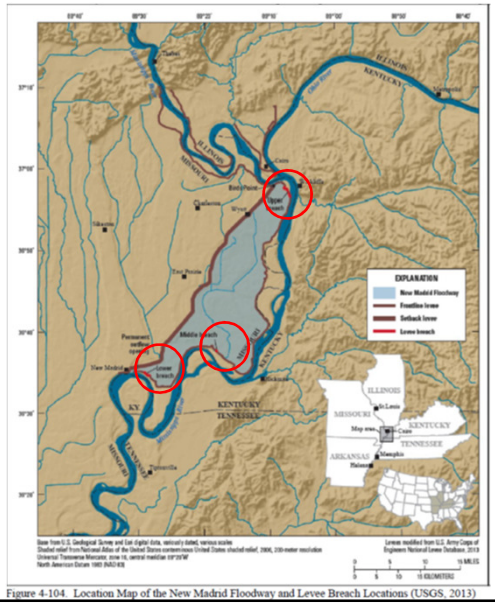

Figure 4-104. Location Map of the New Madrid Floodway and Levee Breach Locations (USGS, 2013)

109

Problem and Data Description

The New Madrid Floodway is located just below the confluence of the Ohio and Mississippi Rivers. This floodway is surrounded by a levee system, which is designed to be activated during major floods. Approximately 9,400 feet of the upper levee was activated on 2 May 2011 just after 2200 hours. Later, two lower sections of the levee were also activated to allow water to drain out more efficiently. Shown in Figure 4-104 is the New Madrid Floodway along the Mississippi River, as well as the levee system. The three locations in which the levee system was breached are shown in red.

Detailed terrain data was obtained for the area inside of the floodway. The grid cell size for this terrain area is five feet. Outside of the floodway the terrain data varied from twenty to thirty foot cell sizes. Surveyed cross section data was obtained from several Corps District offices for the Upper and Lower Mississippi Rivers, as well as the Ohio River. Levee locations (X, Y coordinates), and elevation data were obtained from the Corps' National Levee Database.

Flow data was obtained for the upstream boundaries from USGS gaged locations. A rating curve was used for the downstream boundary condition of the lower Mississippi River 1D reach. Breaching information was obtained from USACEs.

110

Table 4-39. Model parameters for the New Madrid Floodway Breaching Validation Test Case

Parameter	Value
Time step (minute)	2
Governing Equations	SWE
Implicit Weighting Factor	1
Manning's roughness 1D rivers	0.021 – 0.033 main channel 0.080 – 0.200 overbank areas
Upper Levee Breach width (feet)	9,400
Middle Levee Breach width (feet)	690
Lower Levee Breach width (feet)	4,100

111

Figure 4-105. Combined One- and Two-Dimensional HEC-RAS Model of the Mississippi, Ohio, and New Madrid Floodway

112

Table 4-40. Measured and Computed Peak Water Surface Elevations (WSEL)

Location	Computed WSEL (feet)	Observed WSEL (feet)	Difference (feet)
H1	324.47	324.10	0.37
H2	324.51	324.24	0.27
H3	324.64	324.17	0.47
H4	324.65	324.24	0.41
H5	324.46	324.24	0.22
H6	324.48	324.16	0.32
H7	324.57	325.01	-0.44
H8	323.83	323.69	0.14
H9	324.21	323.76	0.45
H10	323.93	323.86	0.07
H11	323.94	323.78	0.16
H12	322.56	322.52	0.04
H13	321.71	321.89	-0.18
H14	323.17	323.09	0.08
H15	323.69	323.14	0.55
H16	322.70	322.70	0.00
H17	321.09	321.63	-0.54
H18	315.00	314.64	0.36
H19	321.44	321.79	-0.35
H20	312.79	313.20	-0.41
H21	313.17	313.45	-0.28
H22	311.90	311.93	-0.03
H23	312.46	312.63	-0.17
H24	311.65	311.60	0.05
H25	311.31	311.36	-0.05
H26	310.97	311.06	-0.09
H27	310.74	310.84	-0.10
H29	310.24	310.24	0.00
H30	310.24	309.80	0.44
H31	309.97	309.74	0.23
H32	310.21	309.71	0.50
H33	309.55	309.00	0.55
H34	309.21	308.84	0.37
H35	310.13	309.47	0.66
H36	310.20	309.52	0.68
H37	306.82	306.40	0.42
H38	310.20	309.68	0.52
		Ave ABS Diff	**0.29**

113

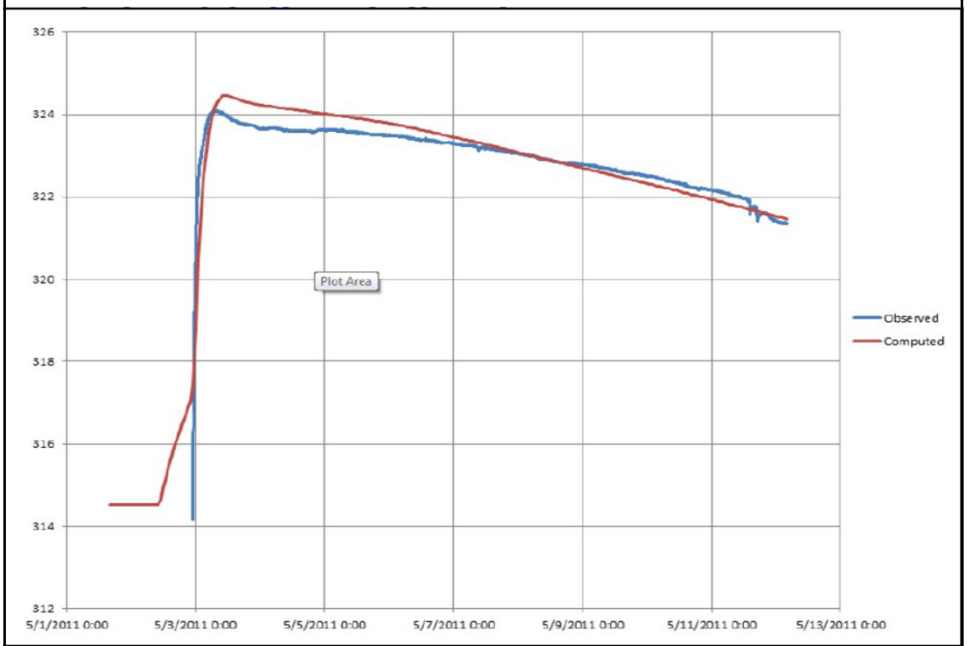

Figure 4-107. Computed versus Observed Water Surface Elevations for Location H1

114

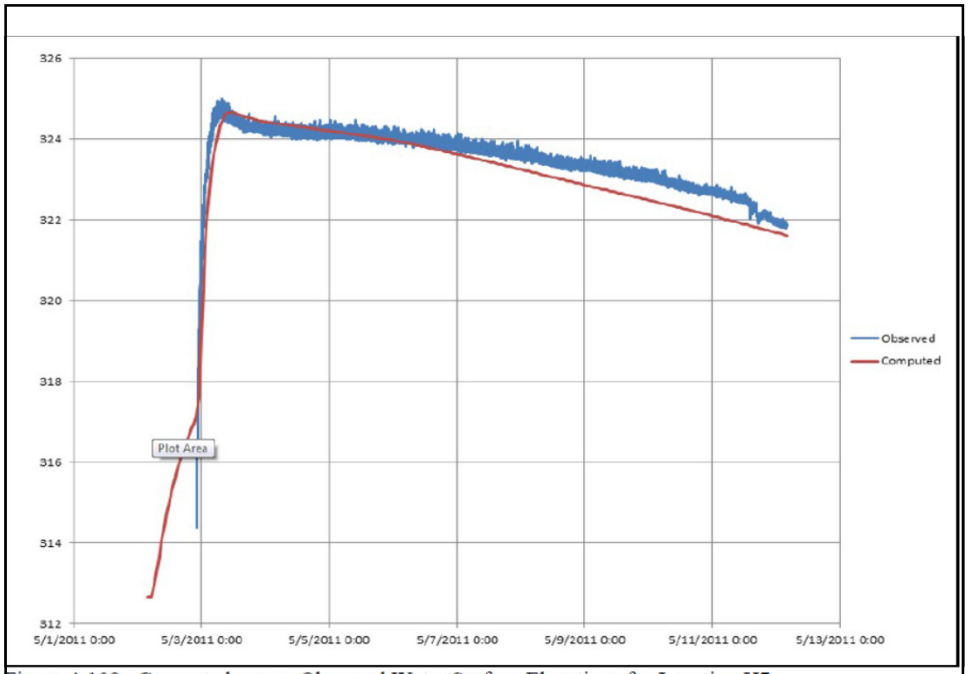

Figure 4-108. Computed versus Observed Water Surface Elevations for Location H7

115

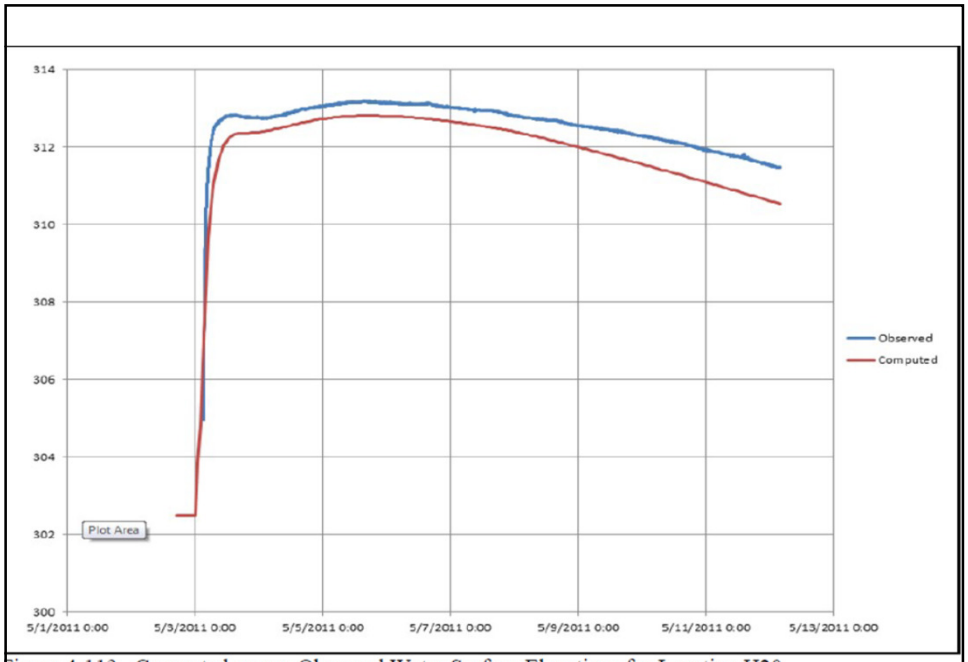

Figure 4-113. Computed versus Observed Water Surface Elevations for Location H20

116